RADIATION FROM AND PANEL RESPONSE TO A SUPERSONIC TURBULENT BOUNDARY LAYER

by

L. Maestrello

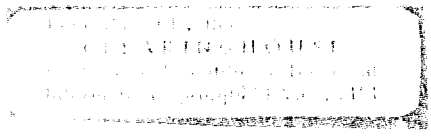

D1-82-0719

RADIATION FROM AND PANEL RESPONSE TO A SUPERSONIC TURBULENT BOUNDARY LAYER

by

L. Maestrello

CONTENTS

SUMMARY

When the convection velocity of the turbulence exceeds the local speed of sound in the medium the coupling of the panel modes to the acoustic field becomes very strong. The structural damping which is usually constant for all modes is overshadowed by the acoustic damping which increases with frequency. For a boundary layer of nearly zero pressure gradient the linear theory is still useful in predicting the panel response and compares well with experiment.

Using Kirchhoff's theorem the acoustic power radiated from a turbulent boundary layer was expressed in terms of the cross spectral density of the pressure field over a rigid plane surface. Computation shows that by using this method the acoustic power level agrees satisfactorily with the measurement.

I. Introduction

A large aircraft in supersonic flight opens new challenges in aeroacoustics, the pursuit of which is vital to advancement in this field. Problems emerge because subsonic experiences are inadequate and it becomes increasingly difficult to define a clear-cut analysis for predicting the response of a panel to a flow field on an aircraft fuselage. The aerothermoacoustic and aerothermoelasticity problems are not part of this investigation. In the present experiment the wall temperature averages around 550 degrees Rankine and the response of the panel is linear, no stress deterioration or stiffness change will occur. Of course, this is a specialized case of nearly zero pressure gradient where the power spectral density technique of generalized harmonic analysis can be used. In the case of larger pressure gradients (shock wave) a more rigorous approach is required, since the flow field leads to instability (flutter) Dowell (1966-1967), Maestrello (1968). It then becomes necessary to use nonlinear plate theory and convenient to use time rather than frequency domain analysis. Even with the simplifications of linear analysis and use of the power spectral density technique, the problem is still complicated due to the necessary inclusion of the pressure resulting from panel motion. The forcing field terms excluding the pressurization effect include the pressure over a rigid wall and that produced by panel motion. The resulting quadratic and inhomogeneity gives rise to a reflection coefficient which imposes additional boundary conditions.

This last development is contained in a report which will follow by Maestrello and McDaid. The present report is concerned with obtaining radiation from a turbulen boundary and panel response to it with emphasis on the coupling of panel modes to the acoustic field which is predominant when the turbulent convection velocity exceeds the local speed of sound in the medium.

These measurements were made on the side wall of the Jet Propulsion Laboratory 20 inch supersonic wind tunnel. The boundary layer is turbulent on the side wall from natural transition. The tunnel was well suited for these measurements partially because the flow conditions are well documented (Coles 1963) and partially because the statistical measurements of the pressure and velocity field are well recognized (Laufer 1961, Kistler and Chen 1962).

II. Experimental Arrangement and Instrumentation

The flow investigated was the side wall boundary layer of the JPL 20 inch supersonic wind tunnel. The tunnel is a continuous flow type utilizing a two dimensional flexible nozzle which provides for speeds up to Mach number 5. A description of the facility with a range of operating conditions is discussed by Laumann (1967). For a brief description with particular emphasis on those features which are most important for velocity and pressure field measurements one may consult Laufer (1961) and Kistler-Chen (1962).

The experiment was arranged to perform three basic measurements: mean velocity profile, wall pressure fluctuations and the response of a simple panel structure. The side wall window was modified to accommodate two identical rigid steel plates which supported the instrumentation required for measurements. One plate contained an array of holes to mount the pressure transducers, Figure 1. Another had a cut-out portion in which the test panel was mounted, Figure 2.

The panel was tested with a static pressure differential loading of 0.06 and 14.0 psi. The operating static pressure of the test section is always below atmospheric pressure. In the case of 0.06 psi pressure differential, a chamber of size 8 x 14 x 6.6 inches was built around the panel to contain the pressure which was kept equal by interconnecting the chamber with the tunnel by a row of holes located downstream from the panel, Figures (2) and (3). Tests with the 14 psi differential were run both with and without this cover.

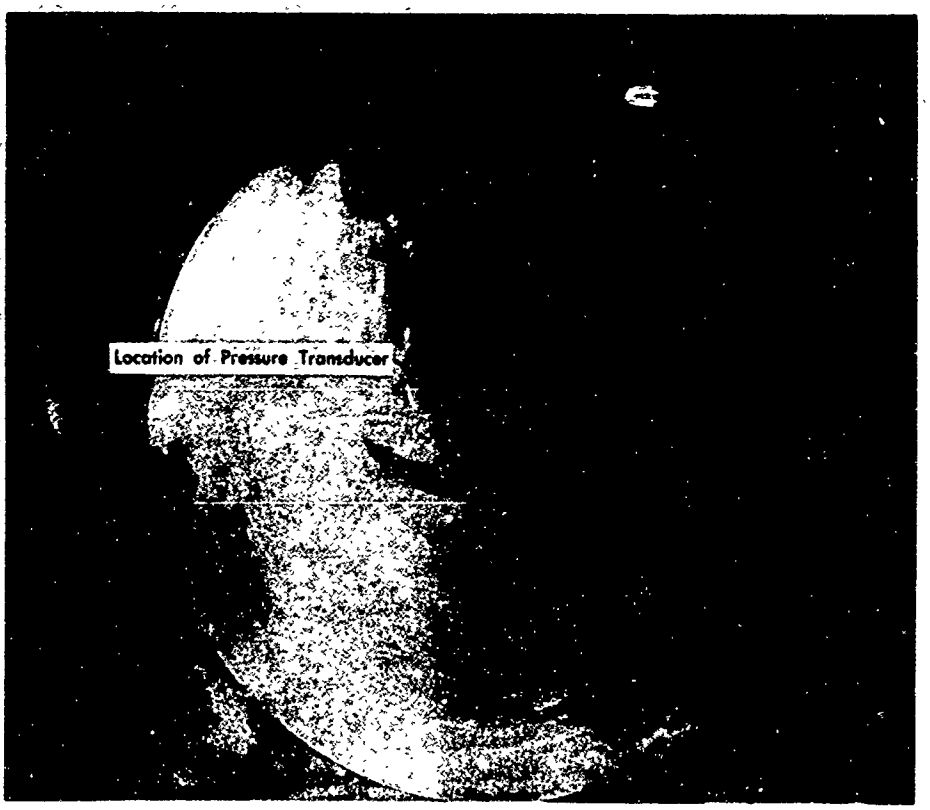

Fig. 1. Transducer mounting configuration.

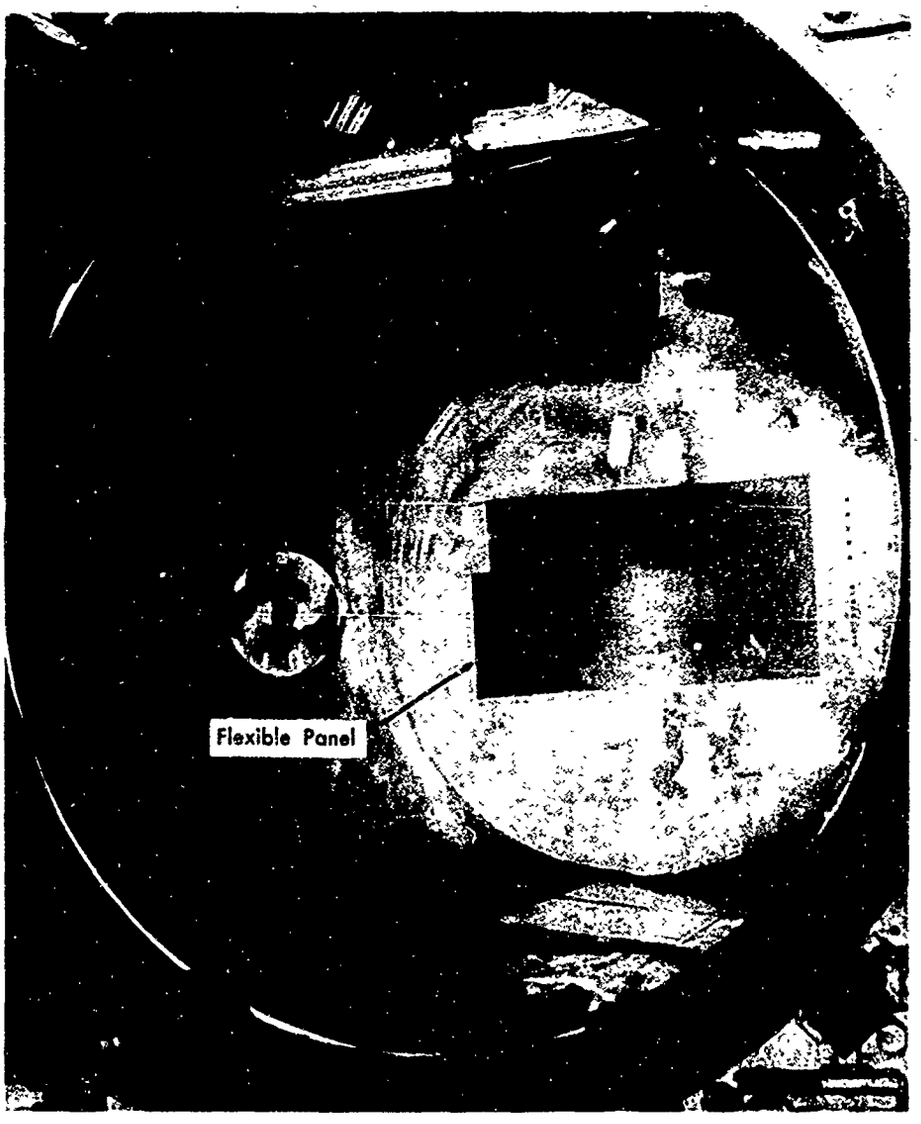

Fig. 2. Test panel.

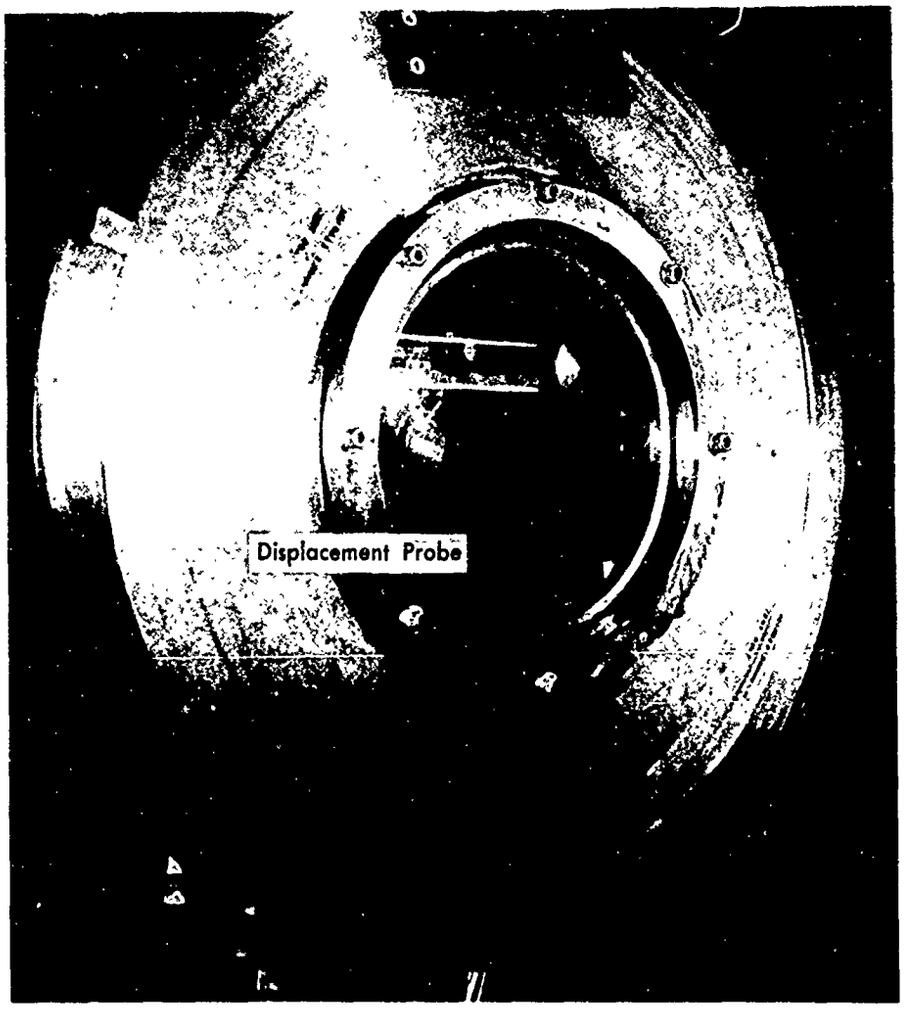

Fig. 3. Panel airlock cover.

The boundary layer on the tunnel side wall is turbulent from a natural transition on a smooth surface. Measurements were made in the region of zero pressure gradient, as well as under conditions of shock and boundary layer interaction. The shock was induced by a 30^{o} wedge mounted outside the boundary layer, off center and to the same side where the measurements were made. This was done to offset the position of the reflected shock from the opposite side. The position of the shock was determined by observing the displacement of a line of tufts, and more precisely, by a static pressure survey. The response of the shock interaction with the panel will be reported separately.

The velocity profile was measured by a standard technique. The wall pressure fluctuations were measured by pressure transducers mounted in the plate shown in Figure 1. The transducers were mounted on a threaded bracket in order to adjust the alignment within ±.0005 inch. The alignment was checked with a micrometer at each transducer location at the tunnel operating pressure. This was the most time consuming operation of the test. If the flushness is not maintained within the tolerance the power spectra would assume a different shape in the lower frequencies.

Two types of pressure transducers were used; one, the conventional lead zirconate titanate made by Atlantic Research and the other a capacitance type made by Photocon Corporation with a sensitive diameter of .060 and .090 inches respectively. This last type of transducer was used to survey the low frequency part of the spectrum because it is less sensitive to vibration than the crystal type. A monitoring survey of the power spectra and cross

correlation was made during the test to insure that satisfactory measurements were recorded on the magnetic tape. In line power spectral density and cross correlation were obtained with a Hewlett Packard wave analyzer and with a Boeing built correlator. The output was recorded on an Ampex FR-1800H 14 channel tape recorder in the FM mode. The main feature of this recorder is that it has a low static and dynamic skewness. Four channels were used for simultaneously recording data for correlation measurements, two channels for the lower frequencies down to the dynamic range of the recorder, and two channels for the higher frequencies. The maximum dynamic range was obtained by splitting each data channel into two tape tracks through phase matched filters to separate the lower and higher frequencies. A high frequency sine wave reference tone was recorded on alternating tape tracks simultaneously with the data for the purpose of correcting time error between data channels used for digital correlation analysis. This technique provides a broad band correlation in both frequency and dynamic range.

The test panel is thin, rectangular, titanium* of size 12 x 6 x .062 inches brazed on all four sides to a 3/4" x 3/4" titanium frame. The brazing is intended to simulate the clamped edge condition. The frame and skin assembly was placed in a vacuum retort using Handy and Harmon braze alloy**.

---

* T1-6AL-4V Titanium alloy containing 6% Aluminum, 4% Vanadium and 90% titanium.

**Braze alloy 70% Ag, 28% Cu, 2% Li.

The retort was placed in a furnace and raised to a temperature of 1450°F. The panel assembly was bolted into the cut-out portion of the plate and made flush with it. The panel displacement was measured with "Photocon" capacitance type displacement transducers mounted on brackets which could slide along a bar and could be set precisely by means of a screw mechanism. The transducer mounting can rotate 360° to allow correlation along the longitudinal and lateral axis. In line power spectra and cross-correlation were taken and then recorded on magnetic tape for 0.06 and 14 psi pressure differentials. Measurements were repeated with damping tape placed on the outside surface of the panel.*

*Two layers of damping tape with surface density of one layer 0.112 lb/FT^2.

III. Measurements and Discussion

Three basic measurements were made: mean velocity profile, wall pressure fluctuation, and the displacement response of a simple titanium panel with clamped edges. Wind tunnels inherently have a certain amount of interference (vibration and sound propagated up or down stream through the boundary layer). Commonly the vibration interference can be bypassed on the measurement of the wall pressure using a capacitance-type transducer. In the present test measurements of the wall pressure fluctuation were rejected below 800 hz due to acoustic interference.

The tunnel vibration will not alter the dynamics of the panel, since it is small compared with that induced by the boundary layer. The fundamental mode (500 and 600 hz for the unpressurized and pressurized case), will be effected by the tunnel interference. The effect is predominant on the fundamental mode and is not expected to be larger than a factor of two.

a) Mean Velocity Profile

The quantities directly measured were the impact pressure, wall pressure and stagnation temperature. The stagnation temperature and static pressure are assumed to be constant throughout the boundary layer. The local static temperature, density and velocities are obtained from the energy and state equations. Therefore, one can assume that the properties of the boundary layer closely approximate the properties of the equilibrium adiabatic flat plate boundary layer.

Measurements made by Coles (1963) using the above assumption over a flat plate, estimated an error in momentum thickness θ of about 2% up to Mach 5. Table 1 lists some of the most pertinent

M_e	U_e (ft/sec)	T_T (°R)	δ (in)	δ^* (in)	θ (in)	$R_\delta \times 10^{-5}$	$R_{\delta^*} \times 10^{-4}$	$R_\theta \times 10^{-4}$	$C_f \times 10^3$	τ_w (lb/ft^2)	$\frac{\mu_e \sigma}{\bar{\mu}}$	$\bar{C}_f \times 10^3$	$\bar{C}_f \bar{R}_\theta$
0.67	745	563	0.84	0.10	0.075	3.22	4.52	2.88	2.06	1.31	0.950	2.20	87.0
1.42	1396	565	0.72	0.131	0.059	2.92	5.30	2.39	2.00	2.06	0.822	2.60	50.9
1.98	1724	563	0.91	0.213	0.070	2.83	6.65	2.17	1.73	1.36	0.697	2.76	41.0
2.99	2078	561	1.33	0.484	0.090	2.52	9.16	1.70	1.35	0.51	0.494	3.00	25.6
3.03	2100	567	1.37	0.445	0.083	4.87	15.77	2.95	1.27	0.89	0.481	2.80	39.8
3.96	2279	570	1.86	0.830	0.097	2.66	11.76	1.37	1.10	0.23	0.348	3.30	15.5
5.08	2404	534	2.30	0.750	0.062	5.43	27.46	2.11	0.54	0.16	0.226	3.20	15.4

Table 1

Boundary Layer Parameters

flow parameters in a supersonic flow at zero pressure gradient. The mean velocity profiles at various Mach numbers were reduced to a constant density form. The method used is based on the work of Coles (1963) in which he assumed that in the sublayer the Reynolds number remained unaffected by the compressibility provided that the density and viscosity are evaluated at mean sublayer temperature. He proposed a simple generalization of the law of the wall such that the similarity functions remained the same as in incompressible flow. The transformed law of the wall is obtained by adopting the Dorodnitsyn type scaling which produces a lateral stretch of the coordinate providing an equivalent incompressible profile. This transformation coincides with the Von Karman hypothesis that the skin friction can be obtained from the incompressible relations by evaluating the density and viscosity of the wall instead of the free stream. An extension of Coles approach has been recently made by Baronti and Libby (1966) and used by Watson and Cary (1967).

Their conclusion was that for an adiabatic flow up to Mach 5 the Dorodnitsyn type transformation can be used to represent the boundary condition such that a universal description of the law of the wall is obtained, but above Mach 5 their method was not successful.

From the law of the wall in the logarithmic region

$$\frac{\bar{U}}{\bar{U}_\tau} = A \ln B \bar{\xi} \qquad \bar{\xi}_f \le \bar{\xi} \le \bar{\xi}_1 \tag{1}$$

where

$$\bar{\xi} = \left(\frac{\bar{C}_f}{2}\right)^{1/2} \left(\frac{\mu_e \sigma}{\bar{\mu}}\right) \left(\frac{U_e}{\nu_e}\right) \int_o^y \frac{\rho}{\rho_e} \, dy. \tag{2}$$

and in the laminar sublayer

$$\frac{\bar{U}}{\bar{U}_\tau} = \bar{\xi} \qquad 0 \le \bar{\xi} \le \bar{\xi}_f \tag{3}$$

$\bar{U}/\bar{U}_\tau = \bar{U}/\bar{U}_e = (\bar{C}_f/2)^{1/2} f(\bar{\xi})$ and $\int_o^y \rho/\rho_e \, dy$ is the Dorodnitsyn variable, $\bar{U}_\tau = (\bar{\tau}_\omega/\bar{\rho})^{1/2}$, C_f = skin friction coefficient, μ = coefficient of viscosity $A = 2.43$, $B = 7.5$ and $\bar{\xi}_f = 10.6$. The ratio $\mu_e\sigma/\mu$ comes from the assumption due to Donaldson (1952) that the Reynolds number associated with the laminar sublayer is invariant. The edge of the boundary layer was selected at a point where the ratio $U/U_e = .995$. The ratio ρ/ρ_e is obtained by using Crocco's relationship for the density profile. The compressible skin friction coefficient C_f is related to the incompressible $\bar{C}_f$ by the following:

$$\bar{C}_f = (\rho_e \mu_e / \rho_\omega \mu_\omega) \qquad (\bar{\mu}/\sigma\mu_e) C_f. \tag{4}$$

The values of C_f, $\bar{C}_f$, $\mu_e\sigma/\bar{\mu}$ and τ_ω are given in Table 1.

A plot of the law of the wall, Figure 4, using the above

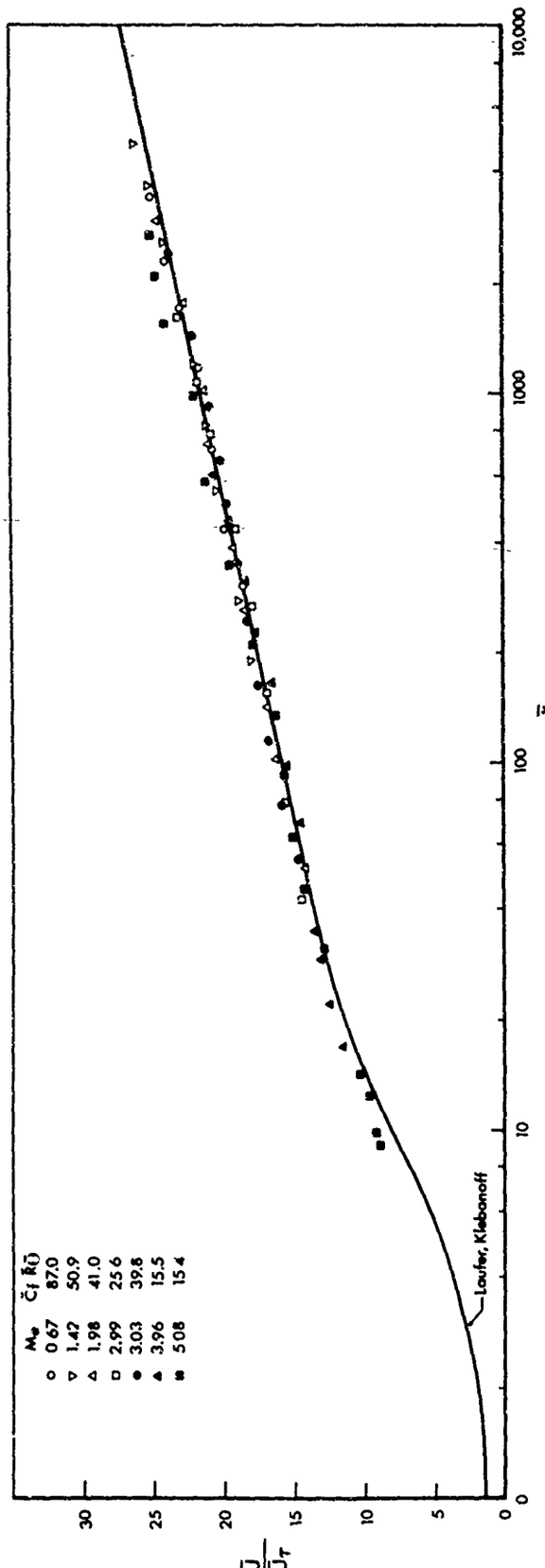

Fig. 4. Mean velocity profile.

transformation compares well with the measurements of Laufer and Klebanoff which were made for an incompressible flow. It can be seen further that the present data transform for an equivalent incompressible boundary layer is in close agreement with the relationship found by Coles, Figure (5), as well as with measurements made by other investigators.

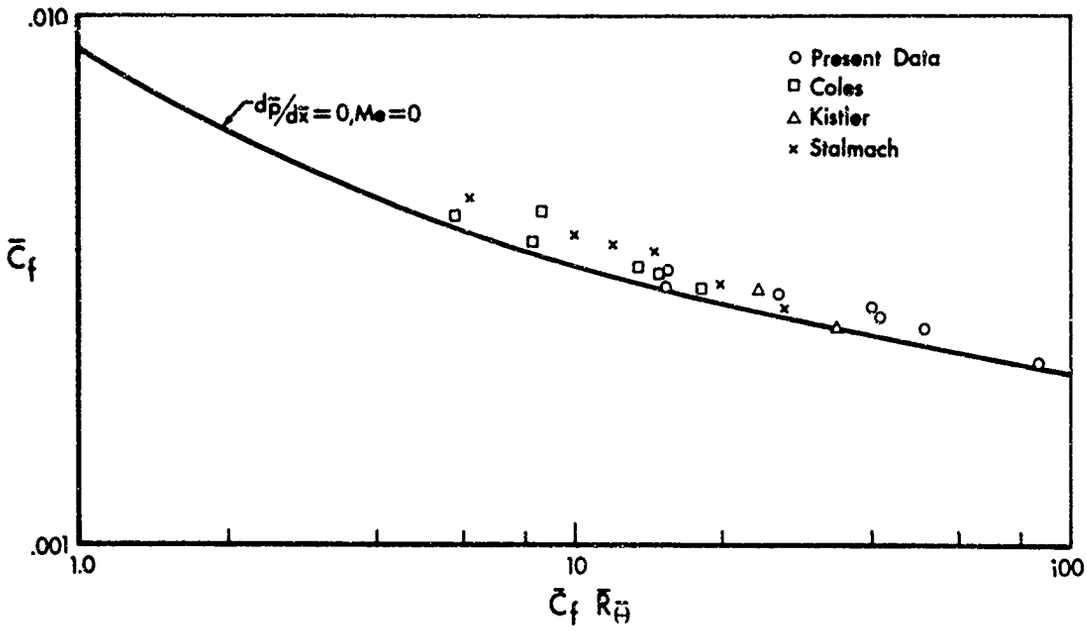

Fig. 5. Local skin friction coefficient for equivalent incompressible flow.

b) Wall Pressure Fluctuation

The problem is to obtain an appropriate description of the wall pressure fluctuation produced by a turbulent boundary layer at near zero pressure gradient. From a spatial and temporal correlation of the pressure field an estimate of the response of the structure can be made.

The structure senses the different components of the pressure as they are swept past the surface at different velocities. Since the panel response behaves like a narrow band filter, a meaningful representation of the field can be obtained with less complexity than would be required to represent the turbulent flow itself. The convected nature of the wall pressure fluctuation can be described by a space-time correlation function. The convected feature is not independent of either spatial or temporal delay on which they are measured but is contingent on both. The decoupled equations for a compressible viscous, heat conducting gas within the framework of the linear theory have three types of disturbance fields. The predominent ones are the vorticity and the entropy modes whose phase velocity is the usual convection velocity. The third type is the acoustic mode in which energy is transported away at the acoustic wave speed. All three modes are independent except at the wall because they are imposed on the velocity and temperature (Kovasznay and Chu 1958).

Laufer (1964) successfully measured the acoustic contribution by recording the density fluctuations along the Mach wave outside the turbulent boundary layer using a hot wire anemometer. Wilson (1959) measured the near and far field of noise radiated by a turbulent boundary layer developed

on a rotating cylinder. Separating the contribution of the acoustic mode at the wall from the other disturbances is more cumbersome because the energy radiated away from the turbulence region represents only a small fraction of the kinetic energy flux of the turbulence and an even smaller fraction when compared with viscous dissipation. However, the wall pressure fluctuation measurement retained the contribution of the acoustic mode as well, and the non-zero correlation integral can be interpreted as energy dissipated acoustically. The sound sources are located away from the surface of higher order than dipoles whose strength is zero at the surface. The sources are equivalent to a quadrupole system. The surface, assumed to be rigid and large, acts as a simple reflector of sound, Doak (1960), Ffowcs Williams and Lyon (1963), Lyamshev (1961), Powell (1960), Meecham (1968), and Kraichnan (1957), apart from the fact that a contribution to the pressure may occur due to the viscous effect, Leehey (1968).

Measurements of the wall pressure fluctuation were made in the range between 0.8 to 200 KH_z using the conventional lead zirconate ceramic disk as well as with capacitance transducers with diameters of 0.060 and 0.090 inch respectively. The normalized power spectra, corrected for attenuation due to the finite size of the transducer (Corcos correction), are shown in Figure 6. The deviation in the shape at lower frequencies may be attributed to extraneous interference* which persisted inside the tunnel and to radiation from the turbulence (this last one is the apparent surface source originated by the source near the surface). The extraneous interference,

*Narrow band spatial correlation measurement for frequency below 0.8 KH_z using capacitance probe transducer (quite insensitive to vibration) shows that the decay of the turbulent pressure has superimposed an acoustic component similar to that shown by Wills (1968).

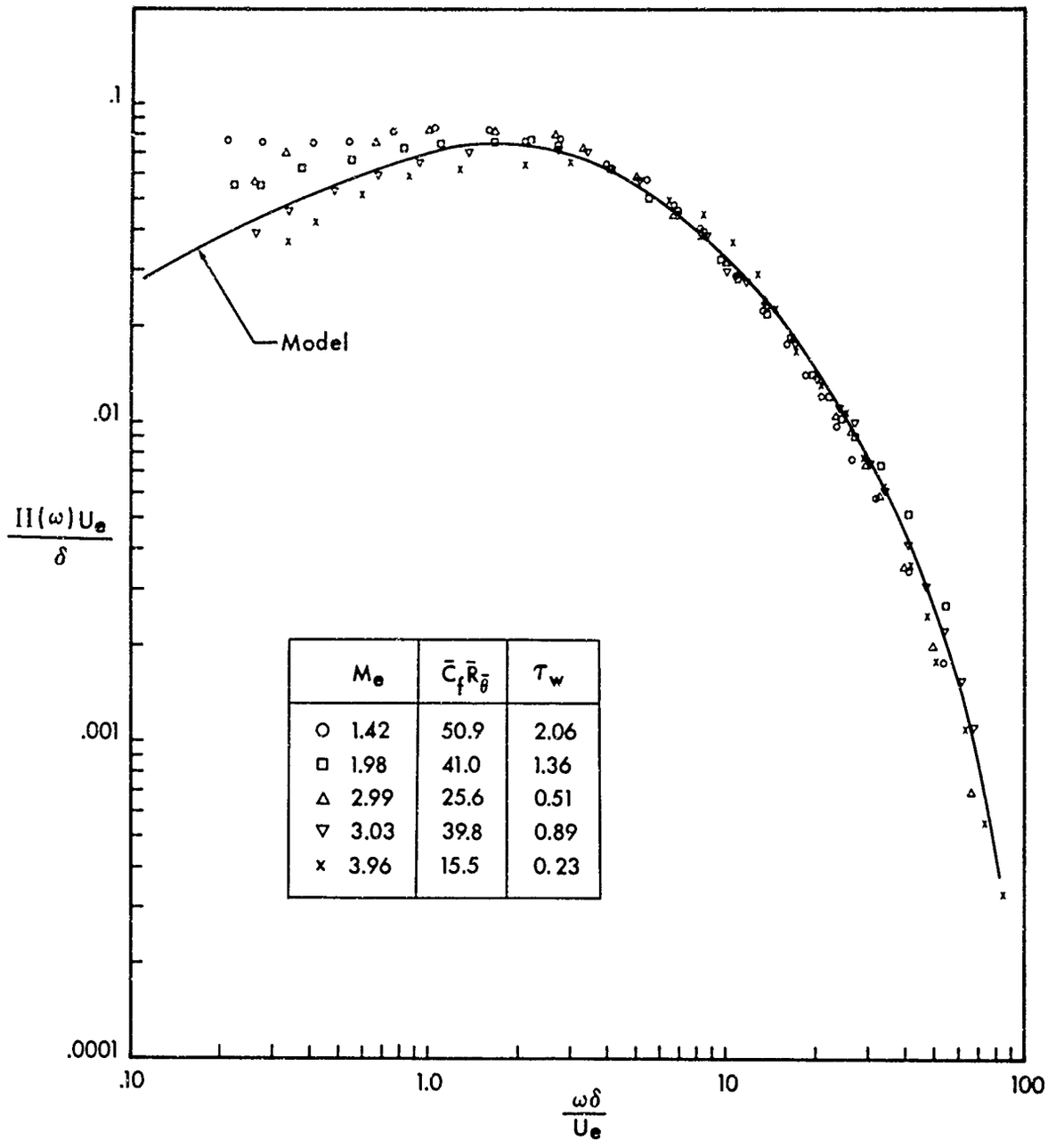

Fig. 6. Power spectral density of the wall pressure fluctuations.

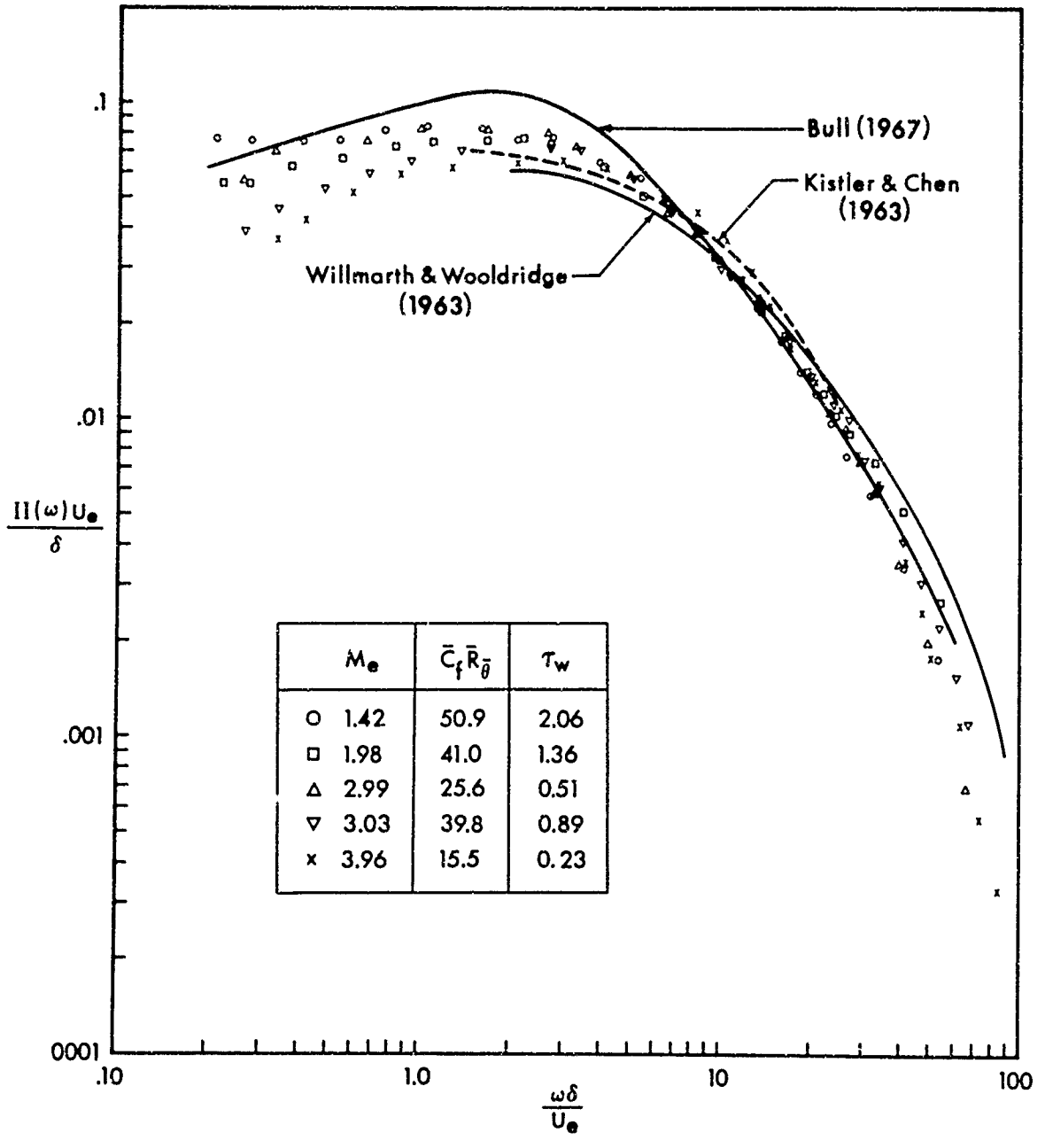

Fig. 7. Power spectral density of the wall pressure fluctuations.

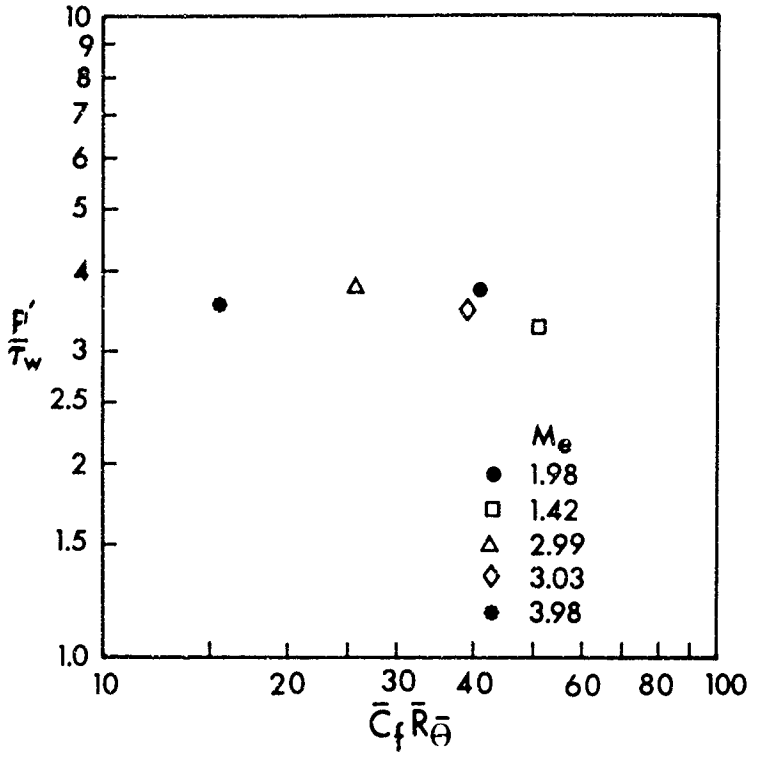

Fig. 8. Pressure fluctuation level.

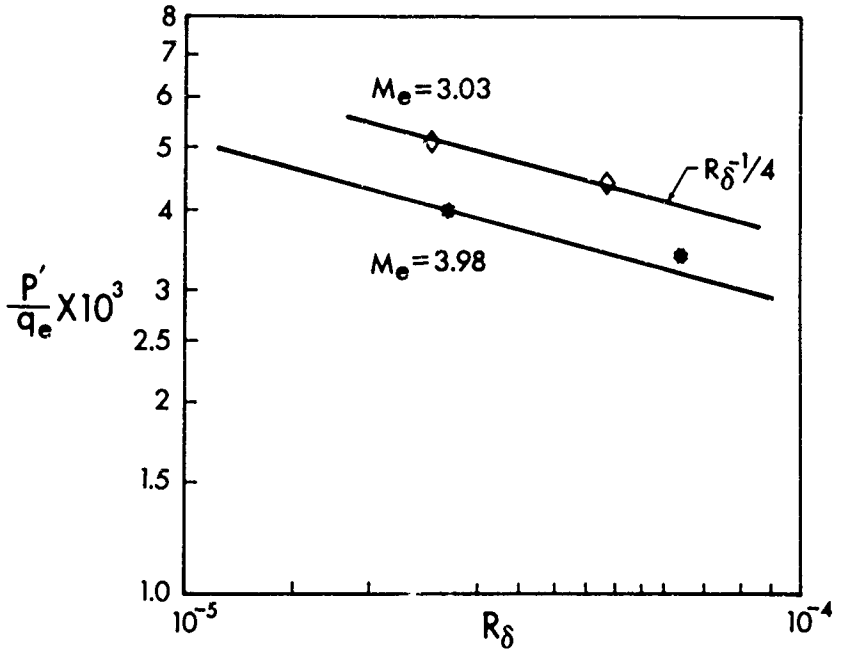

Fig. 9. Variation pressure fluctuation level with Reynold's number.

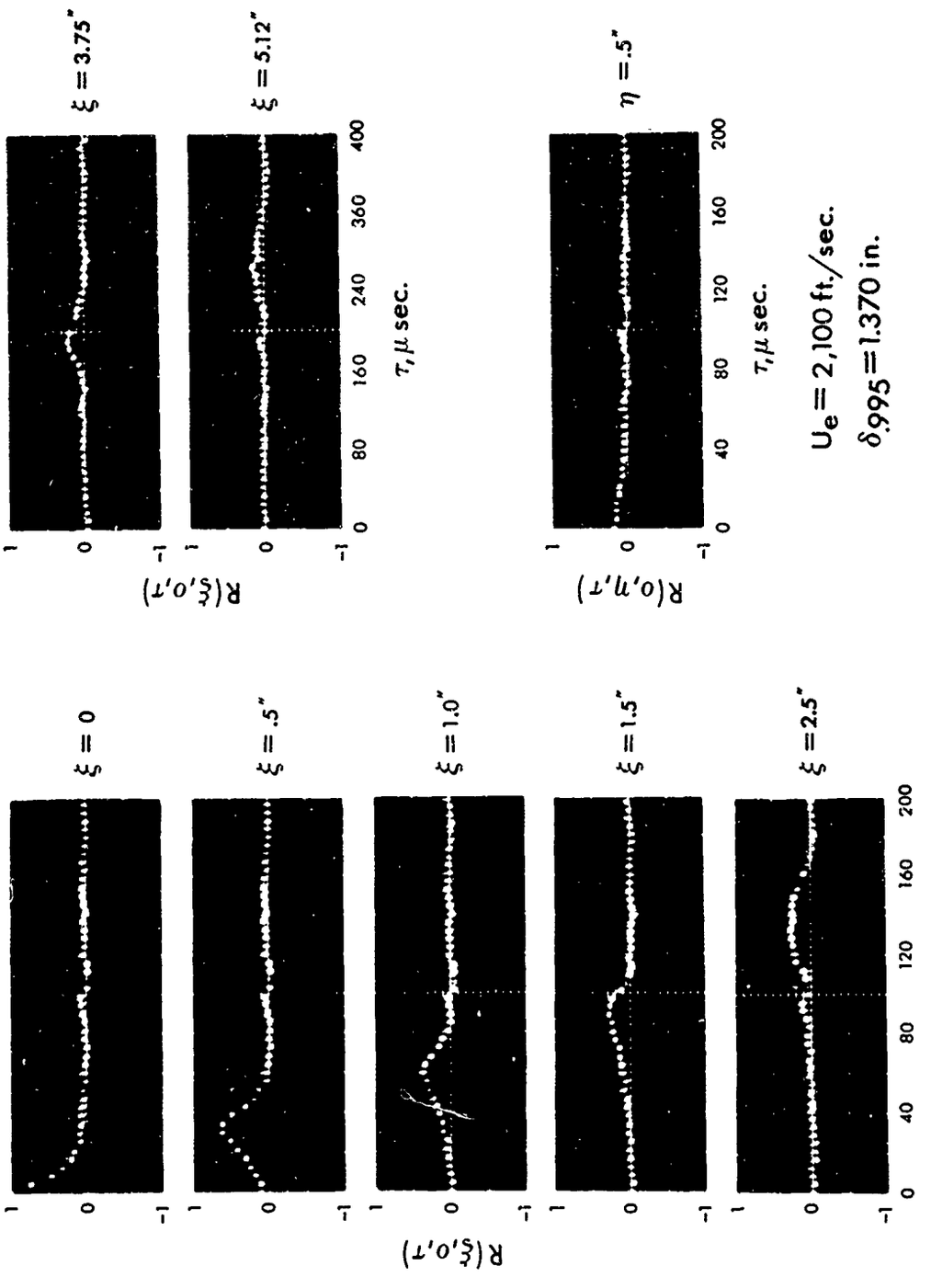

Fig. 10. Space time correlation of the wall pressure fluctuation.

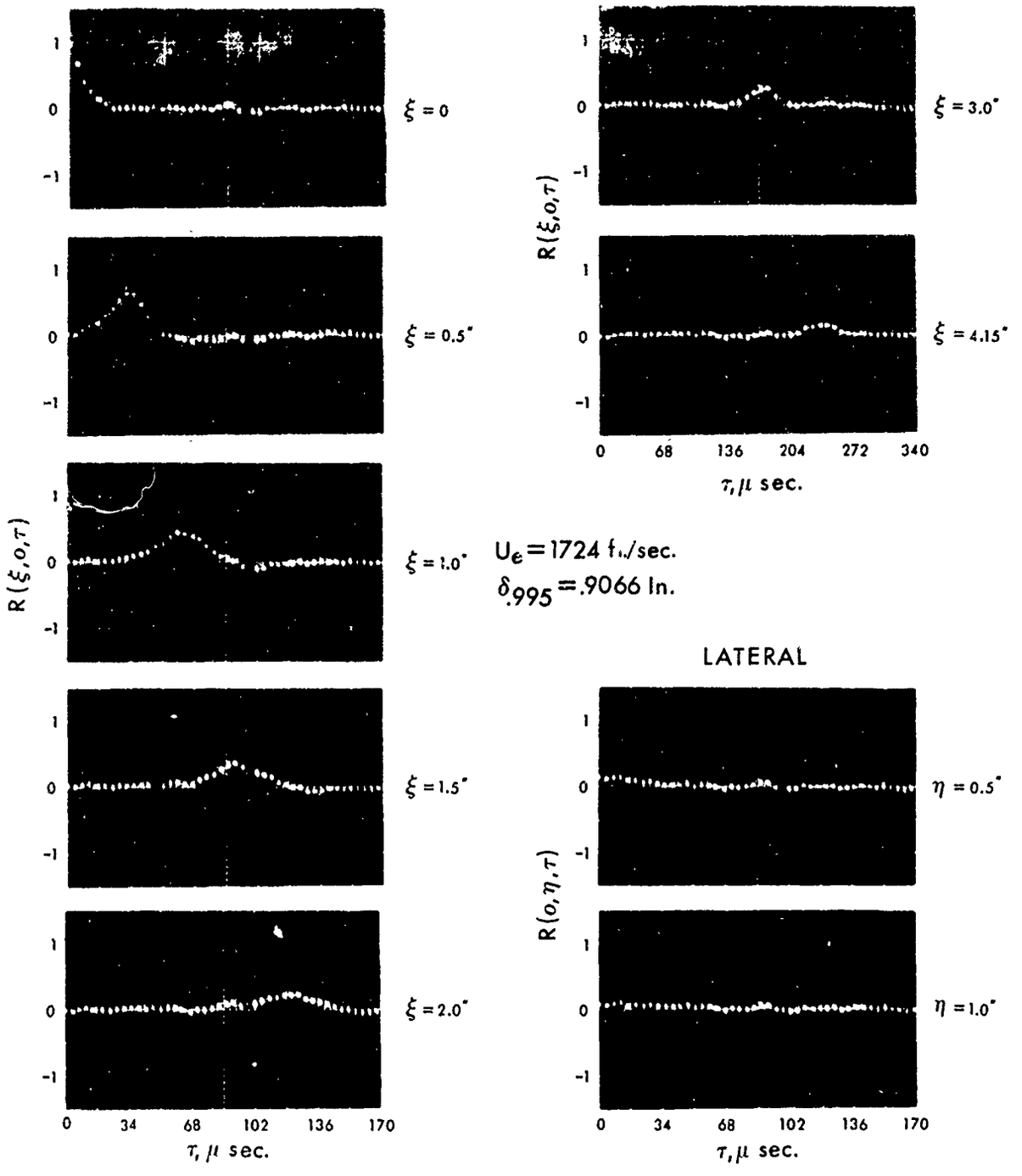

Fig. 11. Space time correlation of the wall pressure fluctuation.

however, masks the radiated noise from the turbulence; this is the reason that the frequency spectra have been truncated at 0.8 KH_z. Lilley and Hodgson (1960) predict that the wall pressure spectral density varies like the square of the frequency at low frequencies for vanishingly small Mach numbers. Ffowcs Williams (1965) shows that for finite compressibility the correlation area varies like the square of the Mach number. The present model of the wall pressure fluctuation retains some of the features contained in the above comments.

The normalized power spectral density (Fig. 6) is similar to that obtained from subsonic flow over a flat plate. It peaks at $\omega\delta/U_e \simeq 2.0$, Bull (1967), Serafin (1963), and Hodgson (1962), show similar behavior (Fig. 7). In contrast for pipe and duct flow the wall pressure spectral density indicates no predominant peak Corcos (1960), Maestrello (1965). In flight, measurements made of the wall pressure fluctuation have a more difficult interpretation because in general there is an apparent pressure gradient, as well as some roughness. Hodgson's measurement, however, over the glider wing produced the typical rolling off spectrum at lower frequency while measurement made on the 727 airplane at higher subsonic Mach number indicates no significant rolling off at the lowest frequencies, Maestrello (1967). Schloemer (1966) from a set of systematic measurements points out that the lower frequency part of the spectral density is sensitive to the pressure gradient. A more extreme case, that is for separated flow Maestrello (1968) indicates a similar observation.

Figs.(6 and 7)show two main eddy structures, the larger scale, faster moving, lower frequency size structure scaled with the boundary layer thickness, and the smaller scale higher frequency, slow moving eddy, scaled with the sublayer thickness. This is also born out from the law of the wall by application of the transform for constant density flow discussed in the previous section.

Further results show that the ratio of the wall pressure with the local wall shear stress p'/τ_w is nearly independent of Mach number, while the ratio of the wall pressure with the free stream dynamic pressure $p'/q_e \sim R_\delta^{-1/4}$. The results are reported in Figs. (8 and 9). Similar results have been previously obtained by Kistler and Chen from measurements made in the same wind tunnel except for about 30% discrepancy in the values of p'. From the figures the product $p'/q_e \times \tau_w/p'$ reproduces the well-known results of the frictional law, the compressible skin friction coefficient decreases as the Mach number increases at a constant Reynolds number.

The broad band space-time correlation curve for separation in the stream direction $R(\xi,0;\tau)$ and in the lateral direction $R(0,\eta;\tau)$ are shown in Figs. (10 and 11), obtained at constant spatial separation and at variable time delay. The cross correlation retained a frequency band-width from $0.5\ KH_z$ to in excess of $100\ KH_z$ with an adequate dynamic range. The longitudinal correlation shows the usual convected feature, slowly losing its coherence, while with the lateral correlation no convection is observed except possibly at large separations where the envelope flares out at small correlation values. The broad band convection velocity corresponds to $U_c/U_e = 0.78$ at $M_e = 1.98$ and $U_c/U_e = 0.72$ at $M_e = 3.03$. It is interesting to point out that for correlation measurements taken at constant spatial separation at a slight angle off the flow direction the convection velocity was slightly greater than the one obtained along the flow direction. This could possibly be explained as disturbances moving with particular orientation for the case of supersonic convection, since it is a propagating wave system. Unfortunately insufficient data was obtained to construct the wave pattern over the surface.

From measurements made of the wall pressure fluctuations, plotted dimensionally in Fig. (6) a model is obtained. The model is of similar form to that reported by this author earlier (1967 and 1968) for a duct flow except it takes into consideration a peaked power spectrum, characteristic of a boundary layer developed over a flat smooth plate at zero pressure gradient. From the figure the power spectrum $P(\omega)$ and the normalized spectrum $\pi(\omega)$ satisfy the following relationships:

$$\int_0^\infty \pi(\omega)\,d\omega = 1 \qquad \int_0^\infty P(\omega)\,d\omega = \langle P^2 \rangle \approx 12\tau_w^2; \quad \frac{\pi(\omega)U_e}{\delta} = \sum_{n=1}^{4} A_n e^{-K_n(\omega\delta/U_e)} \tag{5}$$

where $A_1 = 4.4 \times 10^{-2}$ $\qquad K_1 = 5.78 \times 10^{-2}$

$A_2 = 7.5 \times 10^{-2}$ $\qquad K_2 = 2.43 \times 10^{-1}$

$A_3 = -9.3 \times 10^{-2}$ $\qquad K_3 = 1.12$

$A_4 = -2.5 \times 10^{-2}$ $\qquad K_4 = 11.57$

The normalized auto correlation is

$$R(\tau) = \sum_{n=1}^{4} \frac{A_n K_n}{K_n^2 + (\tau U_e/\delta)^2} \tag{6}$$

The flow considered is semi-frozen, that is with decay in space and time at constant convection velocity U_c. From Eq. (6) using Taylor's hypothesis the longitudinal spatial correlation is:

$$R(\xi) = \sum_{n=1}^{4} \frac{A_n K_n}{K_n^2 + \left(\frac{\xi U_e}{\delta U_c}\right)^2} \tag{7}$$

From experimental observation the lateral spatial correlation suggests

$$R(\eta) = e^{-\eta/\alpha_2\delta} \tag{8}$$

and the normalized cross correlation

$$R(\xi,\eta;\tau) = \sum_{n=1}^{4} \left\{ \frac{A_n K_n \, e^{-|\xi|/\alpha_1\delta} \, e^{-|\eta|/\alpha_2\delta}}{K_n^2 + \left(\frac{U_e}{\delta U_c}\right)^2 (\xi - U_c\tau)^2} \right\} \tag{9}$$

where $\alpha_1 = 50/\bar{C}_f\bar{R}_\theta$, $\alpha_2 = 0.26$.

The longitudinal cross-correlation obtained from Eq. (9) is plotted in Figure (12). The positive isocorrelation contours are symmetric about the line $\xi/U_c\tau$ = constant. Negative isocorrelation contours are also shown. Although the negative correlation coefficients are small compared to the positive, the negative correlation is extended over a larger separation distance.

For a maximum correlation with an optimum time delay there exists a velocity U_c with which the fluctuation patterns are convected downstream. For large separation the convection velocity is obtained from Eq. (9) by:

$$\frac{\partial R(\xi,\tau)}{\partial\tau} = 0 \qquad U_c = \frac{\xi_{max}}{\tau} \tag{10}$$

In this region the maximum-maximorum, the envelope $\exp-|\xi|/\alpha_1\delta$ is quasi tangent to the peak at ξ_{max}/τ. For an incompressible flow the wall pressure correlation is expected to closely satisfy the boundary conditions derived by Phillips (1955) and Kraichnan (1956), that is, the integral

$$\iint_{-\infty}^{\infty} R(\xi,\eta,0)\,d\xi d\eta \tag{11}$$

be zero. The present model, however, takes into account the compressibility effect, and the correlation integral does not vanish.

From the spatial and temporal extension of the wall pressure field one finds it useful to compute the integral scale. The integrals are defined:

$$\begin{aligned} \Lambda_p(\xi) &= 2\int_0^{\infty} R(\xi)\,d\xi \\ \Lambda_p(\eta) &= 2\int_0^{\infty} R(\eta)\,d\eta \\ \text{and } \Lambda_p(\tau) &= 2\int_0^{\infty} R(\tau)\,d\tau \end{aligned} \tag{12}$$

Computation and comparison is given in the table:

	M_e	U_e (Ft/sec)	U_c (Ft/sec)	δ (Ft)	$\frac{\Lambda_p(\eta)}{\delta}$	$\frac{\Lambda_p(\xi)}{\delta}$	$\frac{U_e\Lambda_p(\tau)}{\delta}$	$\frac{\Lambda_p(\xi)}{\Lambda_p(\eta)}$
Bull	0.5	542	445	0.036	0.84	0.40	0.49	0.47
Willmarth & Wooldridge	0.19	204	170	0.42	0.44	0.25	0.35*	0.57
Present Experiment	1.98	1724	1356	0.076	0.85	0.086	0.11	0.11
	3.03	2100	1558	0.11	0.56	0.073	0.10	0.13
Present Model	Given $U_e = 1724$, $U_c = 1356$, $\delta = .076$ $M_e = 1.98$				0.52	0.086	0.11	0.16

The longitudinal scale $\Lambda(\xi)/\delta$ is approximately on the order of the boundary layer thickness except for Bull's result which is one order

*correction applied for revision of data by author.

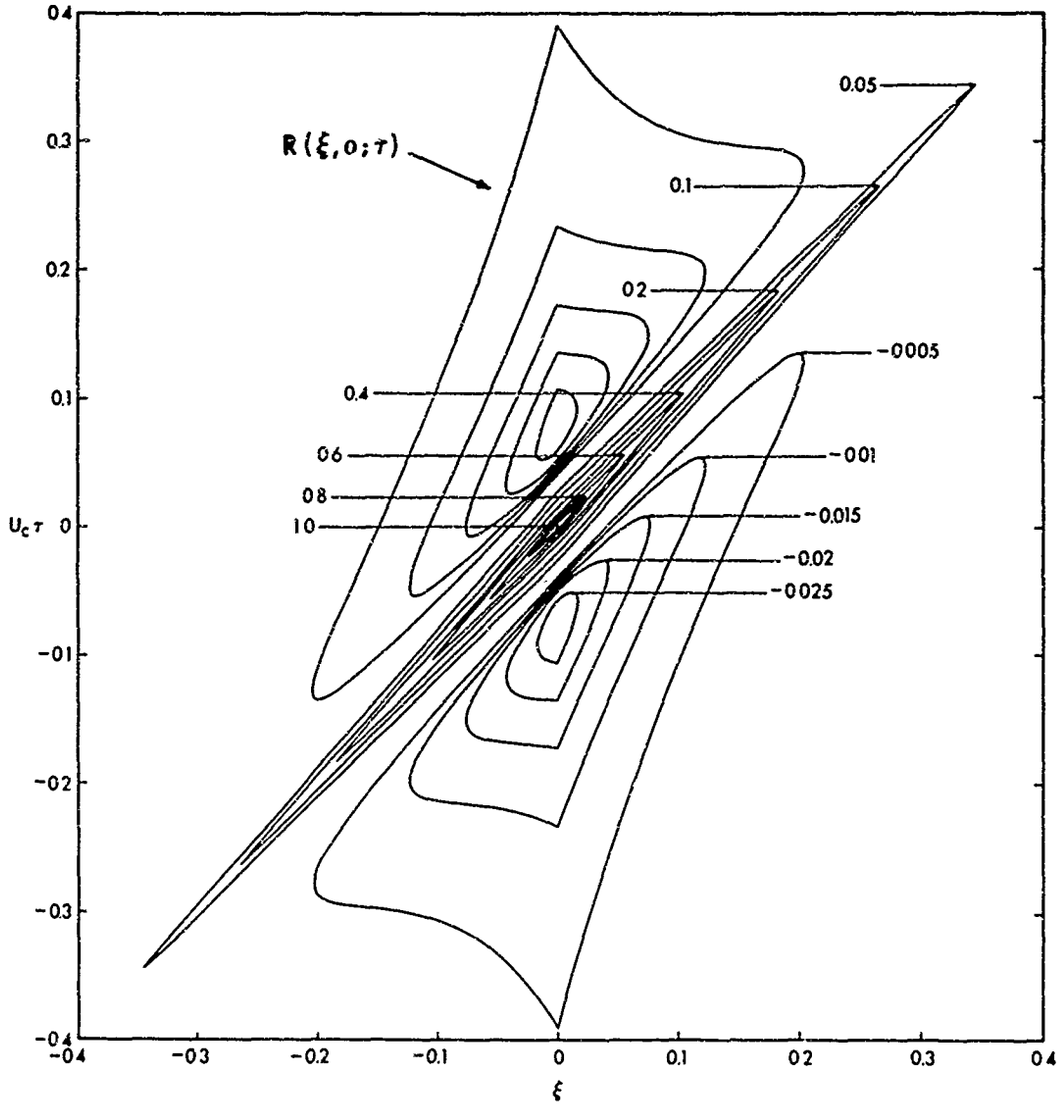

Fig. 12. Longitudinal space time correlation of the wall pressure fluctuation from the model.

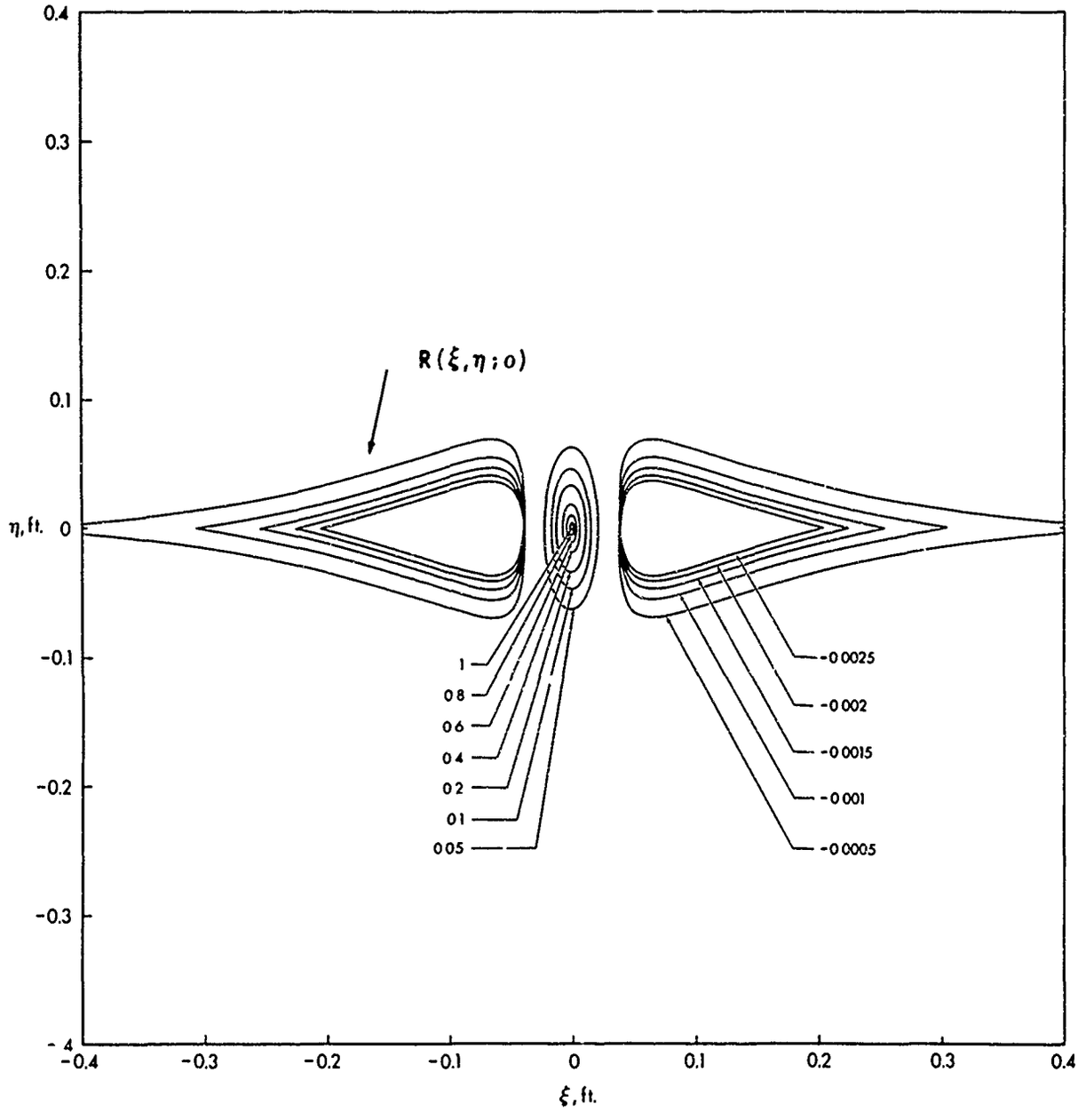

Fig. 13. Broad band spatial isocorrelation contours of the wall pressure.

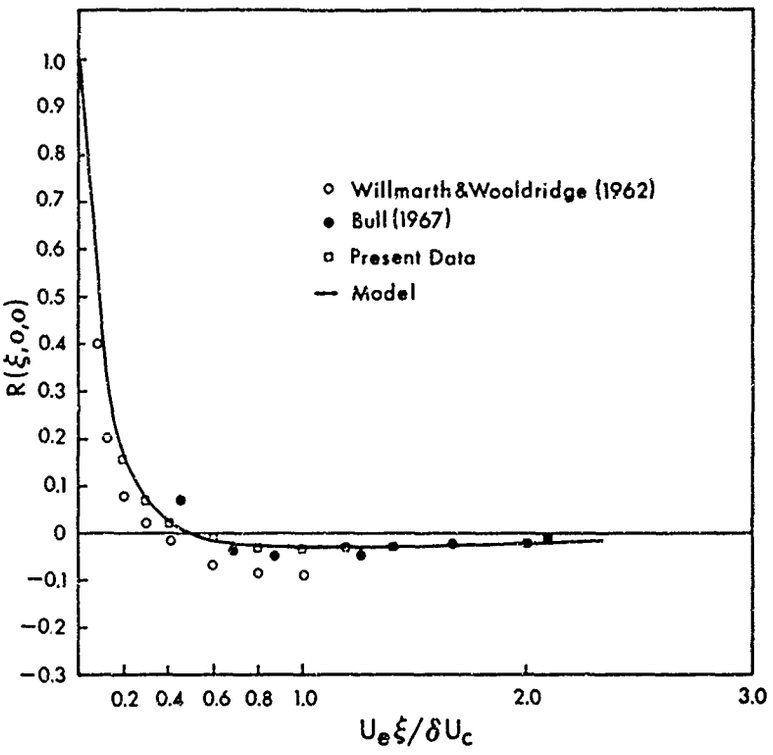

Fig. 14. Longitudinal spatial correlation.

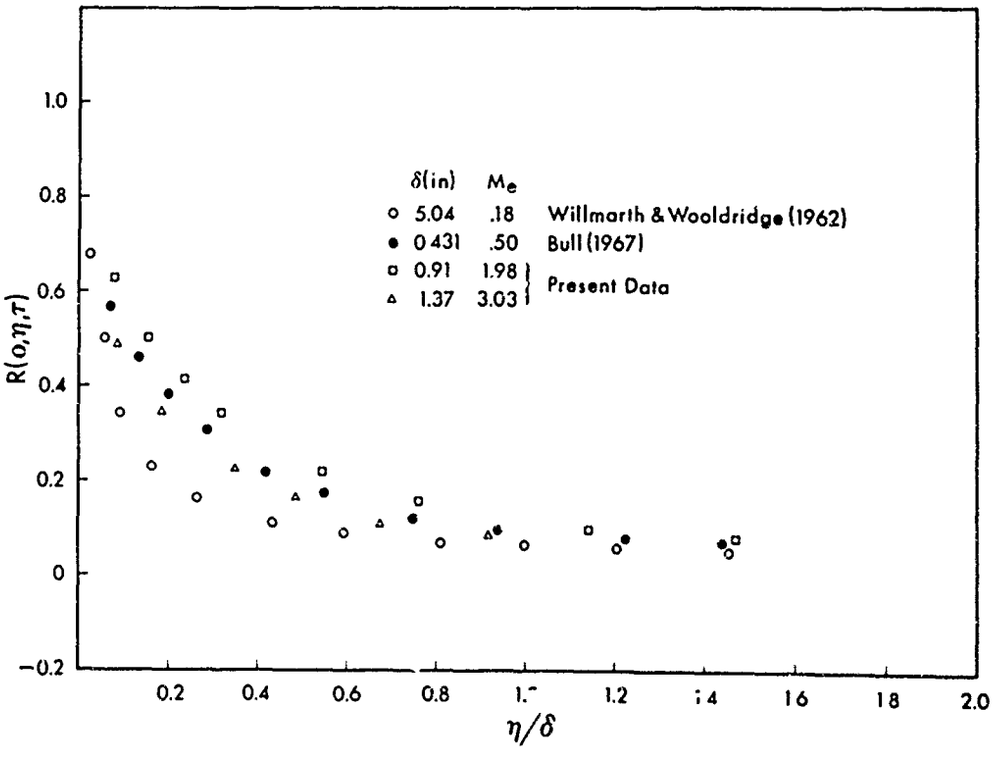

Fig. 15. Lateral spatial correlation.

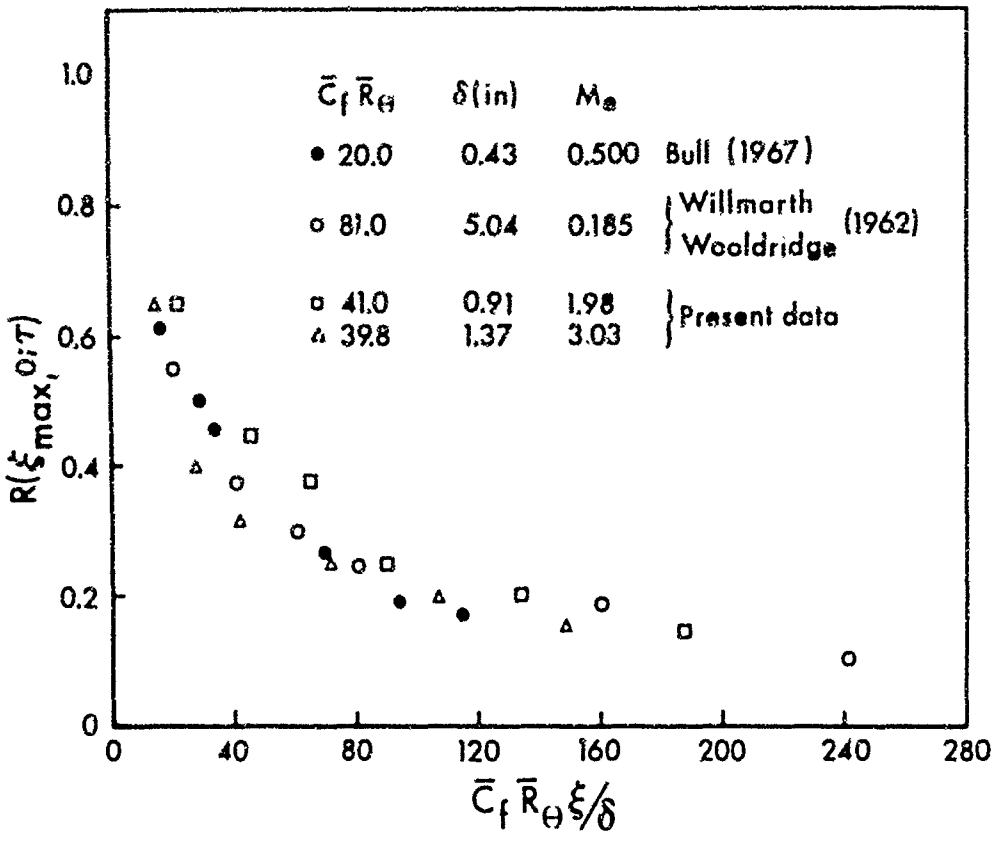

Fig. 16. Envelope of correlation maximum in the direction of flow.

of magnitude smaller. The lateral scale is consistently larger than the longitudinal for all the four experimental results. The ratio $\Lambda_p(\xi)/\Lambda_p(\eta)$ varies from one tenth for supersonic flows to about one sixth tenth for the subsonic. It is of interest to point out that the time integral scale and the ratio of the spatial scales are about equal $\Lambda_p(\xi)/\Lambda_p(\eta) \approx U_e\Lambda_p(\tau)/\delta$. This is evidence that Taylor's hypothesis is quite valid even though error will occur in the extrapolation of the power spectrum $\pi(\omega)$ to zero frequency.

The broad band spatial correlation Fig. (13) shows that for small spacing the correlation field is nearly isotropic but as the separation increases the longitudinal correlation becomes negative due to strong convection while the lateral decays exponentially. Figs. (14 and 15) show the comparison with the measurements and with the model plotted in terms of the normalized parameter $U_e\xi/\delta U_c$ (Eq. 7) using Taylor's hypothesis. Agreement is quite good.

The envelope of the maximum-maximorum is plotted in Fig. (16) using the equivalent incompressible Reynolds number $\overline{C}_f\overline{R}_\theta$ to compare correlation made at different Mach numbers. The pattern of the wall pressure confirms that the increases in separation reduces the higher frequency contribution, the envelope is convex for larger separation. The experimental results show some scatter, however the Reynolds number dependence is consistent. The fact that the convection velocity varies with separation distance is a well-known observation which Favre, Gaviglio and Dumas (1967) termed celerity. Typical narrow band convection velocity is

given in Fig. (17). The ratio $U_c(\omega)/U_e$ almost linearly decreases for large $\omega\delta/U_e$ ratio as indicated in some previous experiments.

It is sometimes convenient to work in the frequency domain rather than in the time domain. From the cross correlation Eq. (9) one obtains the cross spectral density

$$P(\xi,\eta;i\omega) = P(\omega)\ e^{-|\xi|/\alpha_1\delta}\ e^{-|\eta|/\alpha_2\delta}\ e^{-i\omega\xi/U_c} \qquad (13)$$

$$0 \leq \omega \leq +\infty$$

and the wave number spectrum

$$P(K_1,K_2;\omega) = P(\omega)\left[\frac{1/\alpha_1\delta}{(1/\alpha_1\delta)^2 + \left(\frac{\omega}{U_c} + K_1\right)^2}\right]\left[\frac{1/\alpha_2\delta}{(1/\alpha_2\delta)^2 + (K_2)^2}\right] \qquad (14)$$

as ω tends to zero the wave number spectrum varies like U^4. Eq. (14) indicates that the maximum occurs when $\partial P(K_1,\omega)/\partial K_1 = 0$, correspondingly $U_c = -\omega/K_{1\ max}$.

Fig. (18) shows the longitudinal wave number spectra obtained from Eq. (14). The contours show the familiar closed loops previously reported by Bradshaw (1965) in a low speed boundary layer flow. The main difference being that the flow is considered to be semi-frozen while experimentally one can clearly see a variation in convection velocity with spatial separation and time delay.

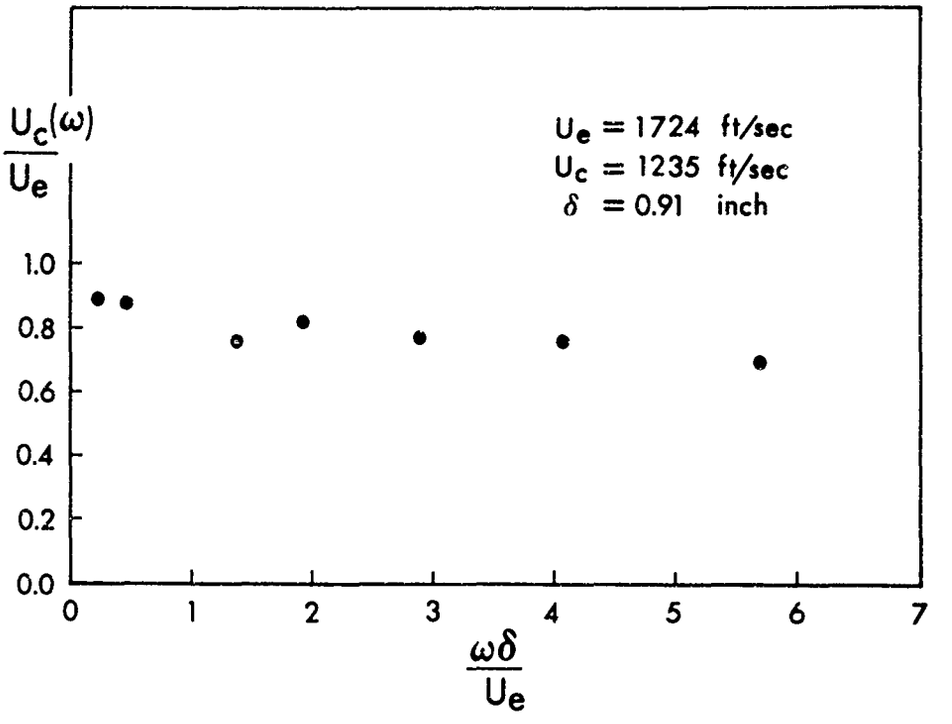

Fig. 17. Narrow band convection velocity.

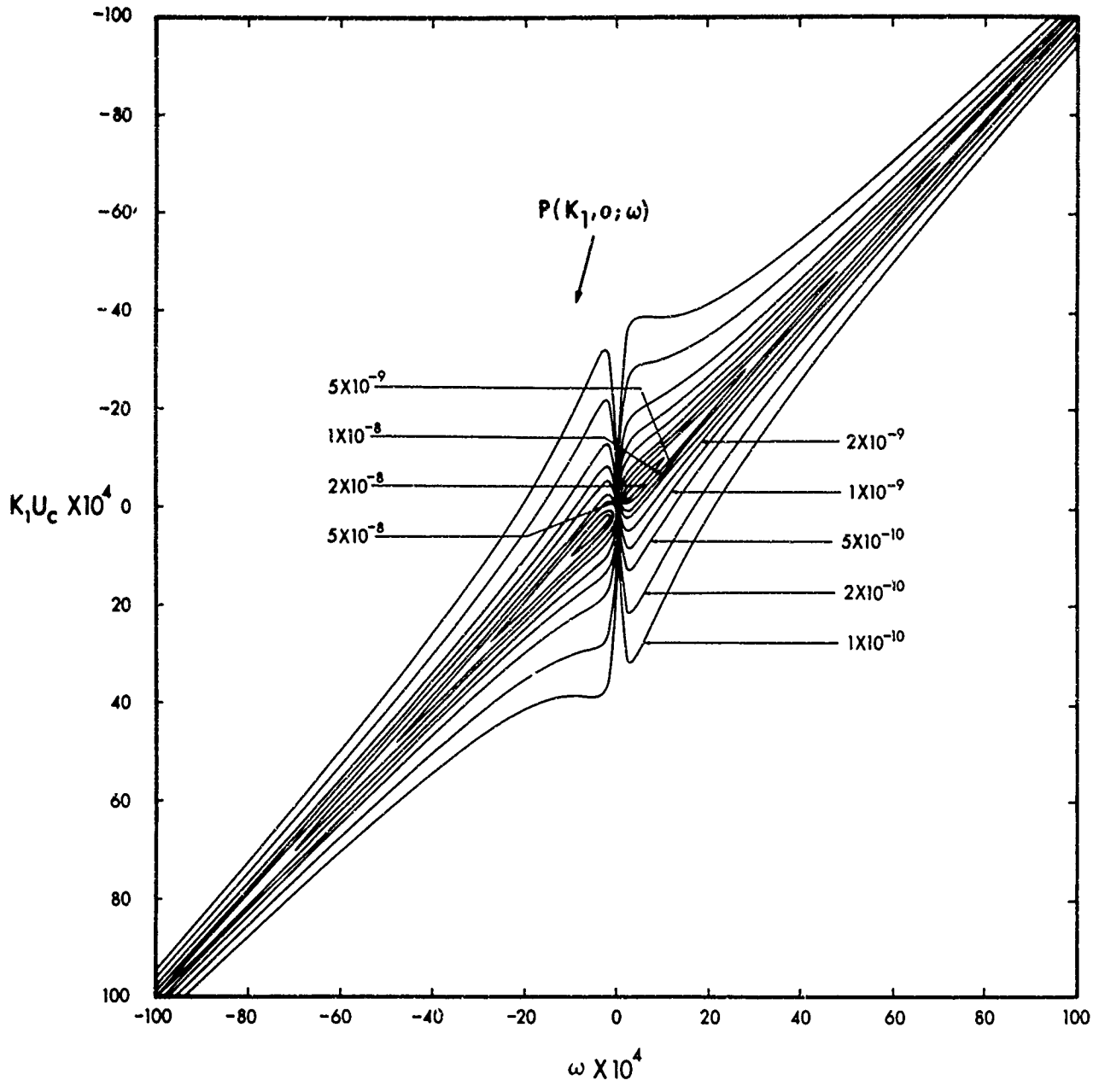

Fig. 18. Longitudinal cross-spectral density.

c) Panel Response

The panel is excited by a steady convected supersonic turbulent boundary layer. The panel deflection is small compared to the skin thickness. It is assumed that the response is linear, stationary and ergodic, therefore the power spectral technique is employed to compute the response, i.e., Crocker, Lyon (1957), Jacobs and Lagerquist (1967), Maestrello (1968), Wilby (1967) and White, Cottis (1968). It is assumed that the plate motion does not modify the turbulent boundary layer. However, the forcing function should contain both the pressure over a rigid wall and that induced by the panel's own motion. In supersonic flow the pressure induced by the panel motion cannot be ignored as in the case of low speed flow, because the supersonic convection velocity excites strong coupling modes to the acoustic field. The spectrum response is mainly controlled by acoustic damping. The pressure due to the panel motion is comprised of waves of subsonic and supersonic velocities. In the subsonic region the damping becomes purely imaginary, the effect is to increase the effective mass of the panel which tends to reduce the resonant frequencies as well as the response, while in the supersonic region the damping is associated with the energy radiating field.

The equation that describes the pressure on the surface is the well-known Kirchhoff solution. Neglecting the viscous term and the terms that are nonlinear in the surface response velocity and taking into account that surface pressure is twice that of the pressure away from the surface, and applying separately the real and image of the boundary layer system from Ffowcs Williams (1966), one can write:

$$\begin{aligned} P(\underset{\sim}{x},t) &= 2T_{+} + 2P_{+} - 2P_{v+} \\ 0 &= 2T_{-} - 2P_{+} - 2P_{v+} \end{aligned} \qquad (15)$$

where

$$T_{\pm} = \frac{1}{2\pi} \frac{\partial^2}{\partial x_i \partial x_j} \int_{v\pm} T_{ij}(\underset{\sim}{y},\ t - \frac{r}{c}) \frac{d\underset{\sim}{y}}{r}$$

$$P_{+} = \frac{1}{2\pi} \frac{\partial}{\partial x_n} \int_{s} P(\underset{\sim}{y},\ t - \frac{r}{c}) \frac{d\underset{\sim}{y}}{r}$$

$$P_{v+} = -\frac{1}{2\pi} \int_{s} \bar{\rho} \frac{\partial v}{\partial t} [\underset{\sim}{y},\ t - \frac{r}{c}] \frac{d\underset{\sim}{y}}{r}$$

Summing the real and image pressure:

$$P(\underset{\sim}{x},t) = 2(T_{+} + T_{-}) - 4P_{v+} \tag{16}$$

when the surface is rigid

$$P_{rigid}(\underset{\sim}{x},t) = 2(T_{+} + T_{-}) \tag{17}$$

At low speed flow the term involving the pressure due to the panel motion is usually neglected since the mass is negligible and the acoustic damping is small. In supersonic flow, the panel radiates sound in the form of Mach waves, weaker in strength due to inhomogeneity in the wave number components but with loss factors sometimes exceeding unity, Maidanik (1966). The measurements made of the displacement spectra show that the higher frequency modes are heavily damped unlike the panel excited by subsonic flow. Figure (19) shows the total damping factor of a 12 × 6 × .062 inch titanium panel with clamped boundaries excited by a turbulent boundary layer at Me = 3.03. The bandwidth Δf is evaluated at the modal half power point. The dotted line is typical of experimental damping for a panel excited by low speed flow. The deviation from this

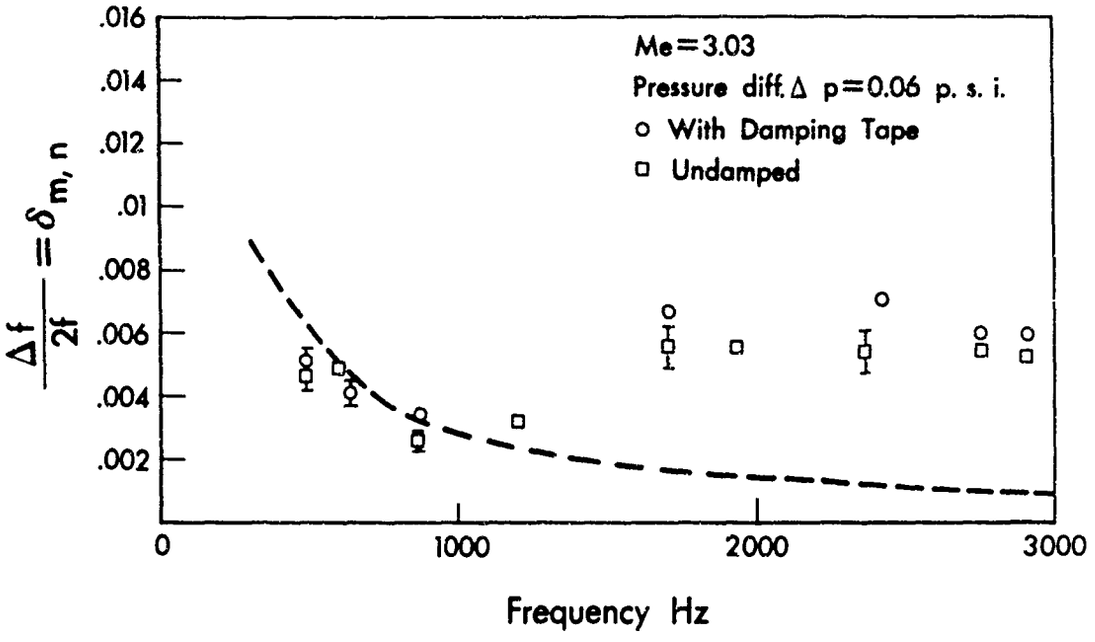

Fig. 19. Damping factor.

curve at higher frequencies is attributed to the wave number components becoming supersonic. The effect of damping tape on the panel is not as significant as might be expected from the low speed case.

Typical displacement spectral densities are shown in Figs. (20, 21 and 22) for a static pressure differential of 0.06 psi and Fig. (23) for a static differential of 14 psi. For the spectra taken at 0.06 psi the panel is enclosed in a cavity Fig. (3) while the spectrum taken at 14 psi the panel radiates into open space. As expected the damping factor is higher when the panel radiates into open space, Strawderman (1967), Pretlove (1964). The broad-band displacement space time correlation measured along the panel centerline in the direction of flow for pressure differentials of .06 and 14 psi are shown in Figs. (24 and 25). For the pressurized panel the response is mainly due to coincidence. The ratio between the wave velocity in the panel and that of the turbulent convection velocity is $\frac{U_{cp}}{U_c} = 0.73$ while for the 0.06 psi pressure differential the broad-band cross correlation shows that the wave velocity of the panel is far below that of the turbulent convection velocity of the pressure field, $\frac{U_{cp}}{U_c} = 0.29$. This suggests that the fundamental mode predominates in the latter case, contribution also results from the modal frequencies of the unpressurized case being lower.

The contribution of the closed cavity on the motion of the panel is small when the depth of the cavity is larger than one-half the larger panel dimension, Pretlove (1964), Dowell-Voss (1963), as in the present test. The main effect is on the damping rather than the panel resonant frequency, negligible interaction is expected between the fluid and the plate. In the case of small cavity depths, however, the principal effects on the

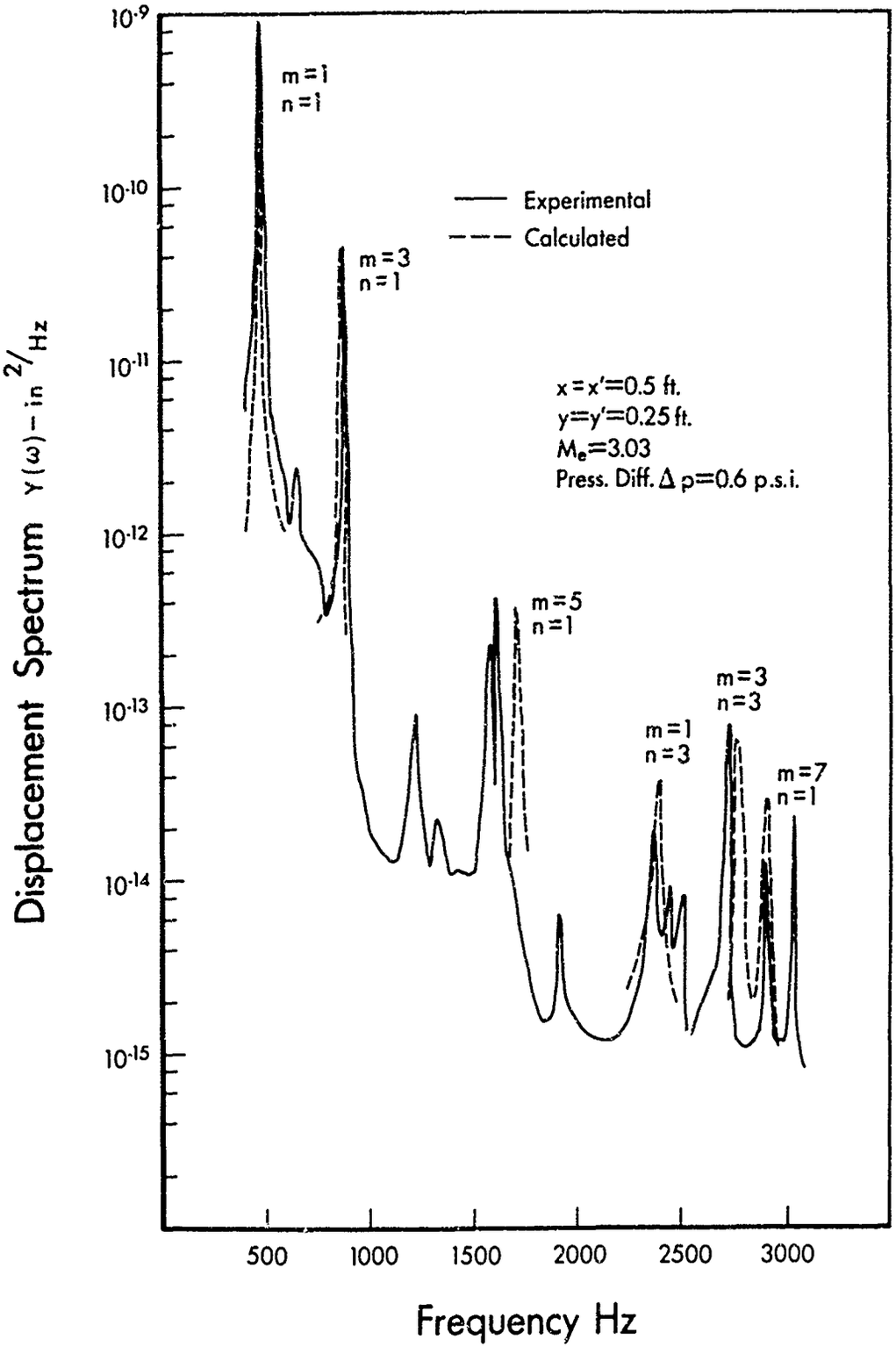

Fig. 20. Displacement spectral density.

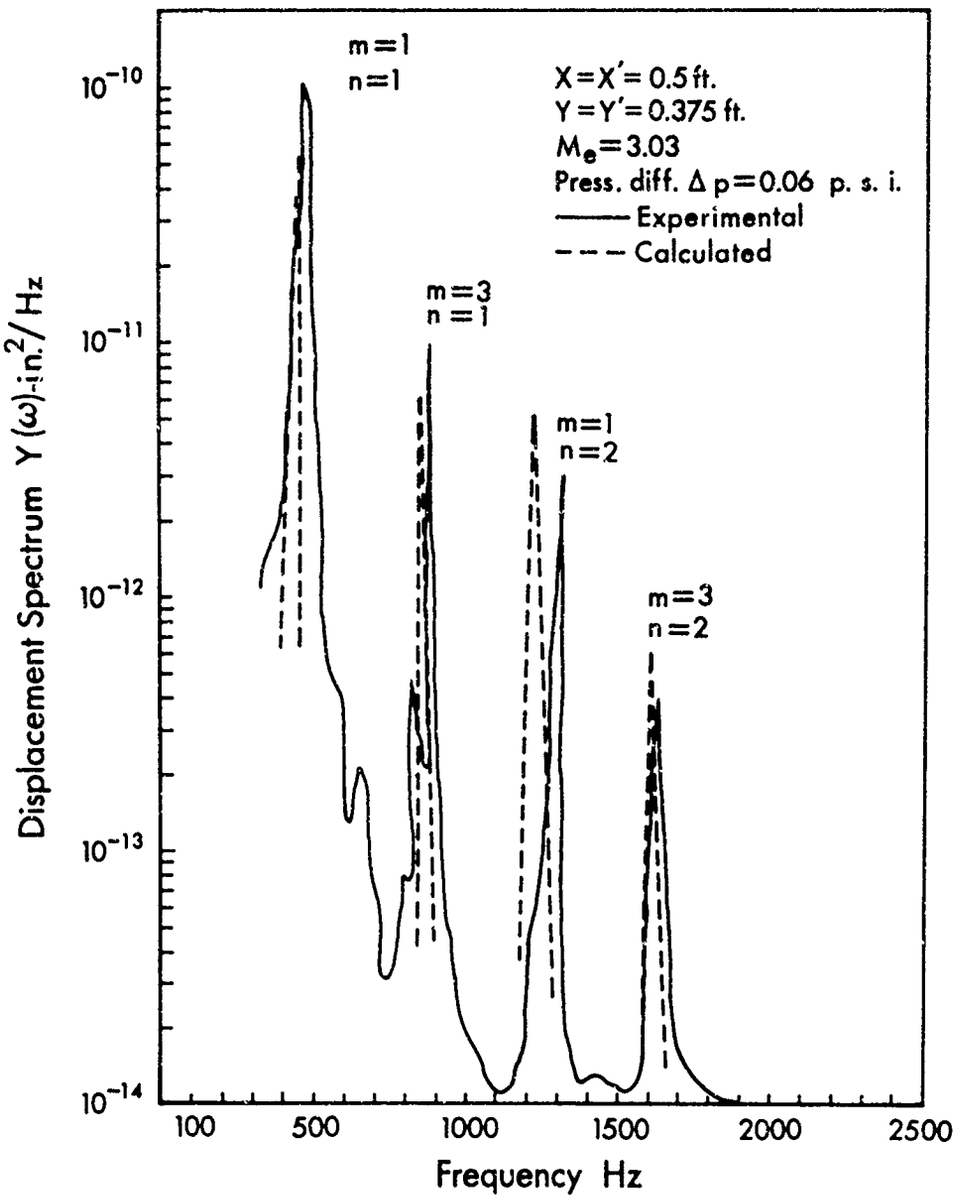

Fig. 21. Displacement spectral density.

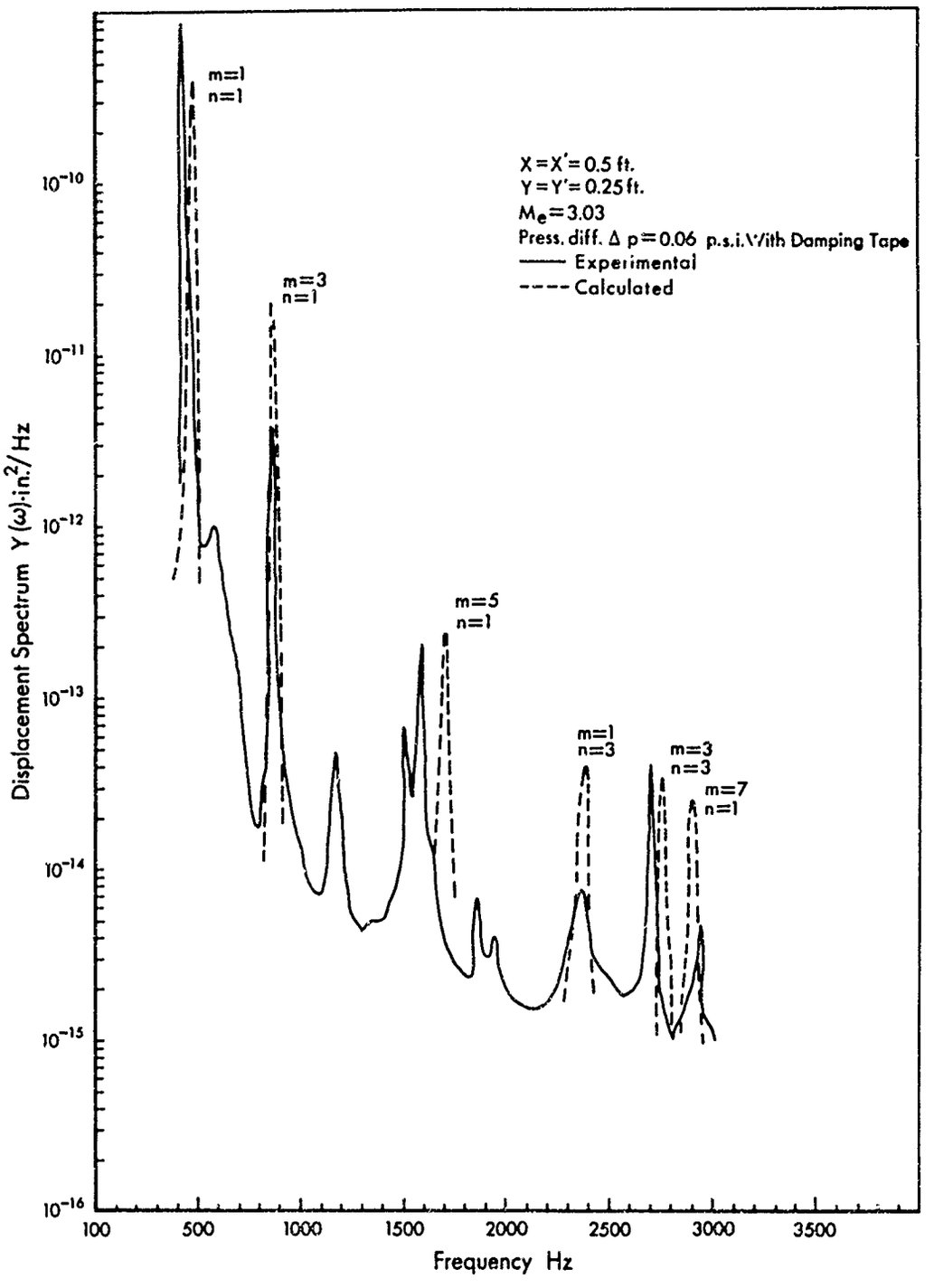

Fig. 22. Displacement spectral density.

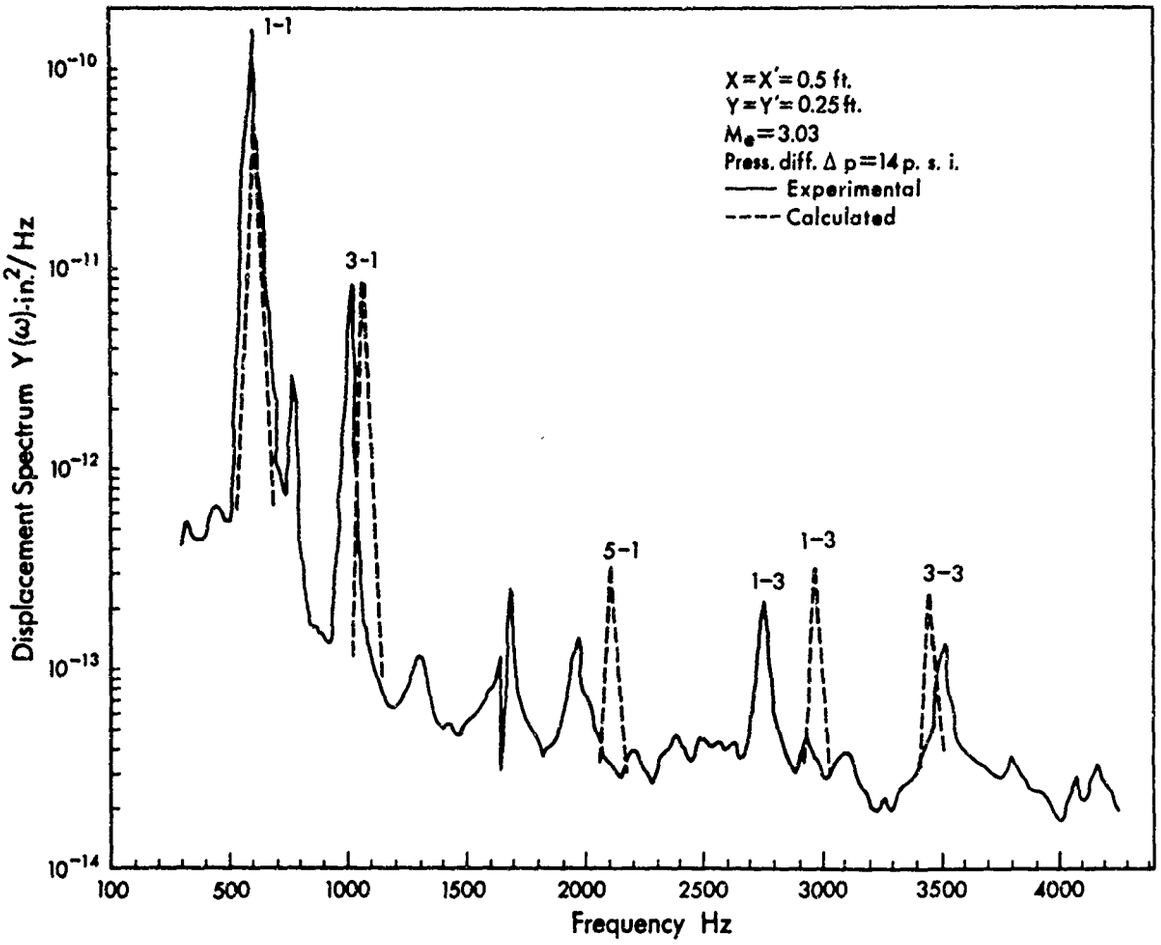

Fig. 23. Displacement spectral density.

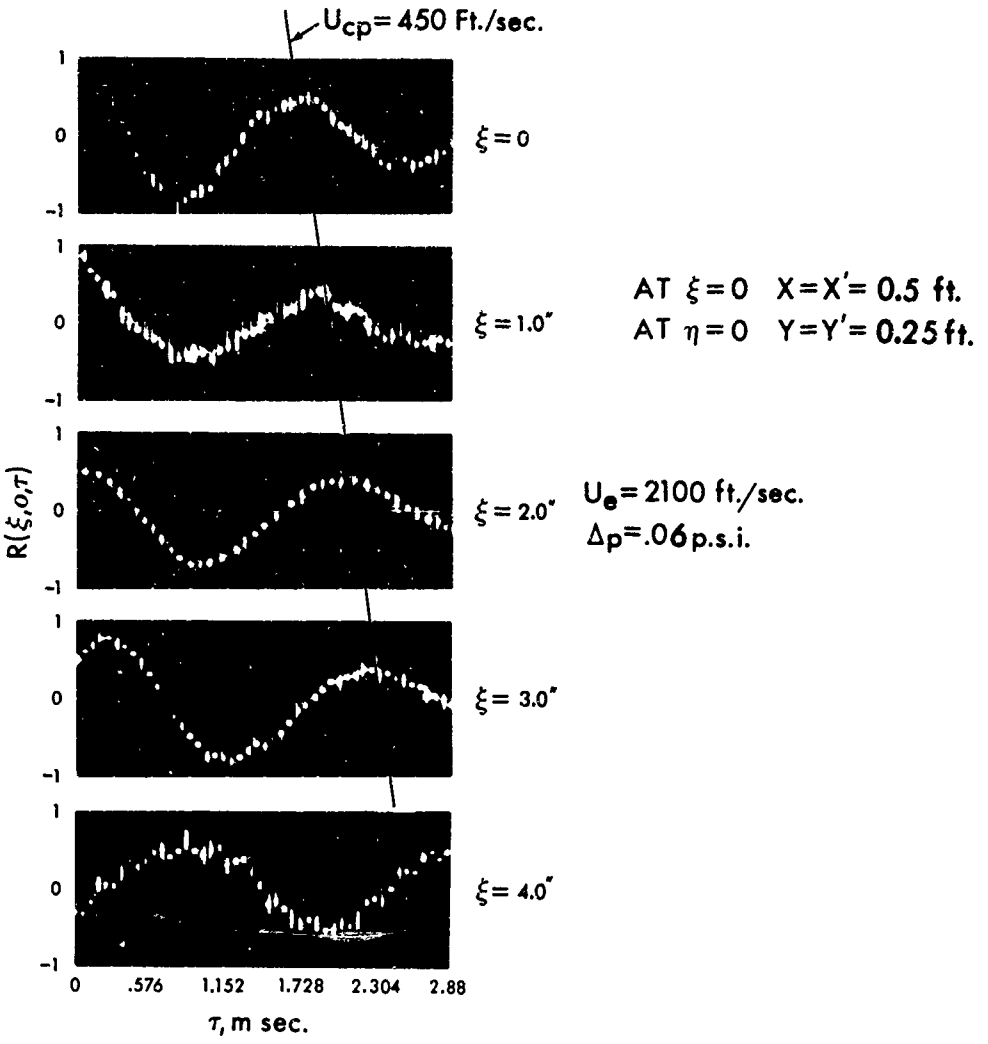

Fig. 24. Broad band space time correlation of panel displacement.

fundamental and symmetrical modes will be that of an aerodynamic spring, whereas for the antisymmetric modes only the aerodynamic virtual mass effects exist.

Fig. (20) shows some alteration in mode shape, for example the experimental $m = 5$ $n = 1$ mode is strongly coupled to the $m = 3$ $n = 2$ mode. This last mode should be zero for an orthogonal system at the measured position. A similar effect is seen in that the $m = 2$ $n = 1$ and $m = 4$ $n = 1$ are also non-zero.

Fig. (26) shows the data of Fig. (25) replotted on the $\xi - U_{c_p} \tau$ plane. The isocorrelation contours are inclined at approximately 45 degrees indicating a convected nature and the decay feature of the correlation coefficient.

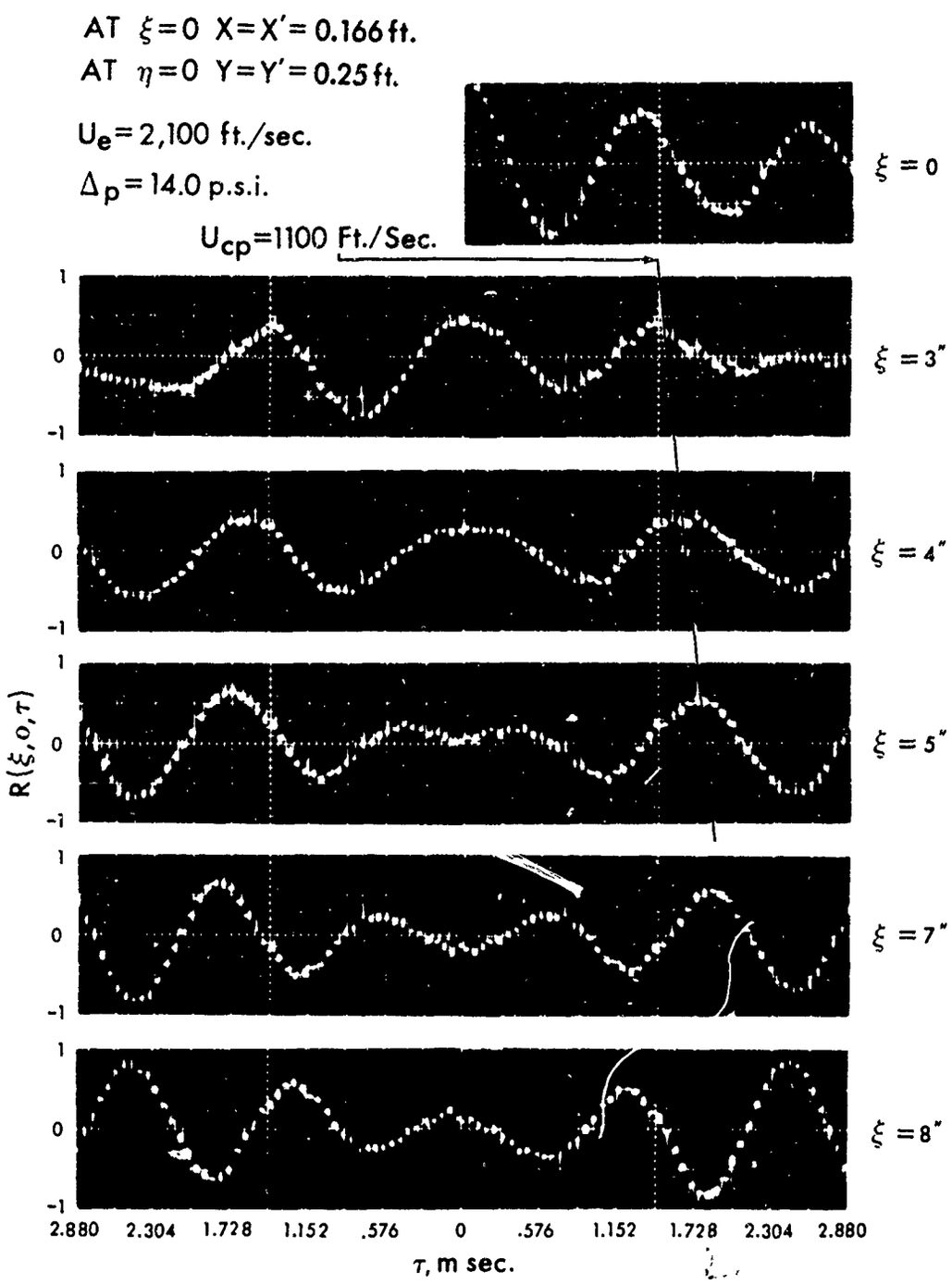

Fig. 25. Broad band space time correlation of panel displacement.

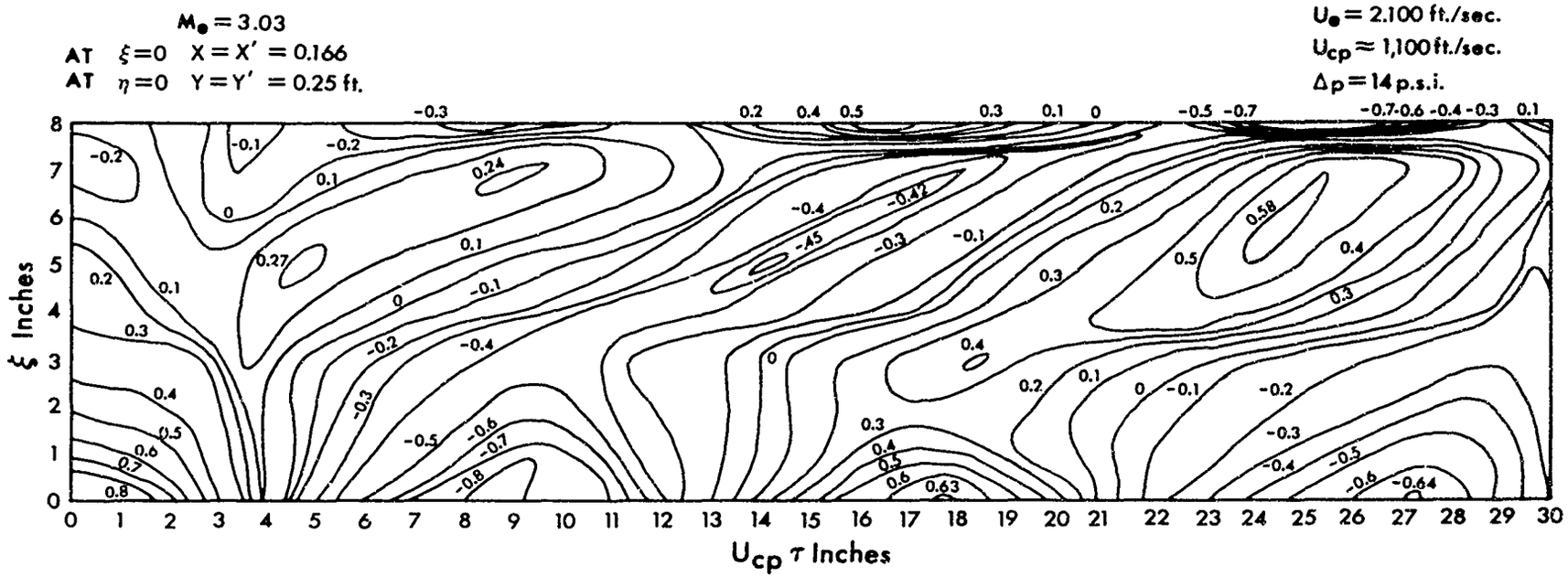

Fig. 26. Longitudinal isocorrelation contours of panel displacement.

IV. Analysis of the Panel Response

The response of linear system to random forcing function is obtained utilizing Green's functions. The system (panel) is excited by random pressure such as the turbulent boundary layer, therefore the assembled average or correlation of the surface displacement is expressed in terms of the correlation of the pressure field,

$$\overline{y(x,y,t)y^*(x',y',t')} = \int_{-\infty}^{t} dt_o \int_{-\infty}^{t'} dt_o' \int_o^a dx_o \int_o^b dy_o \int_o^a dx_o' \int_o^b dy_o' \tag{18}$$

$$g(x,y,t|x_o,y_o,t_o)g^*(x',y',t'|x_o',y_o',t_o')\langle f(x_o,y_o,t_o)f^*(x_o',y_o',t_o')\rangle$$

where the forcing function for the boundary layer pressure field is given by Equation (9).

$$\overline{f(x_o,y_o,t_o)f^*(x_o',y_o',t_o')} = \overline{p^2} \tag{19}$$

$$\times \left\{ \sum_{j=1}^{4} \frac{A_n K_n e^{-|x_o-x_o'|/\alpha_1\delta} e^{-|y_o-y_o'|/\alpha_2\delta}}{K_n^2 + \left(\frac{U_e}{\delta U_c}\right)^2 \left[([x_o - x_o'] - U_c[t_o - t_o'])^2 + (y_o - y_o')^2\right]} \right\}$$

It can be shown (Dyer 1958) for a plate with arbitrary boundary conditions, the Green's function satisfies the classical plate equation and can be represented by:

$$g(x,y,t|x_o,y_o,t_o) = \sum_{m,n} \frac{\phi_{mn}(x,y)\phi_{mn}(x_o,y_o)}{\omega_{mn}M} e^{-a_{mn}(t - t_o)} \tag{20}$$

$$\sin \omega_{mn}(t - t_o)U(t - t_o)$$

where $U(t - t_o) = 1$ where $t_o \leq t$

and $U(t - t_o) = 0$ where $t_o > t$

where $\phi_{mn}(x,y)$ are the normalized eigenfunctions, a_{mn} is the modal damping and ω_{mn} is the damped resonance frequency. The normal mode satisfied the following equation

$$B(1-i\eta)\nabla^4 Y_{mn} + M\frac{\partial^2 Y_{mn}}{\partial t^2} + \beta\frac{\partial Y_{mn}}{\partial T} = 0 \tag{21}$$

where B is the bending stiffness, M is the mass per unit area of the plate, β is the viscous damping coefficient and η the loss factor associated with hysteretic damping.

The modal damping

$$a_{mn} = \frac{\omega_{mn}}{\eta}\left[\left(1 + \frac{\eta\beta}{\omega_{mn}M} + \eta^2\right)^{\frac{1}{2}} - 1\right] \tag{22}$$

and

$$\omega_{mn}^2 = \frac{B}{M}\Gamma_{mn}^4 - a_{mn}^2 \tag{23}$$

where Γ is the eigenvalue of Eq. (21).

Equation (18) involves the product of two doubly infinite sums, the cross-product of the two modes (m,n) and (p,q) is:

$$\overline{Y(x,y,t)Y^*(x',y',t')} = \frac{\overline{p^2}g^2}{M^2} \sum_{m,n}\sum_{p,q} \frac{\phi_{mn}(x,y)\phi_{p,q}(x',y')}{\omega_{mn}\omega_{pq}} \int_0^t dt_0 \int_0^{t'} dt_0' \Bigg\{ e^{-a_{mn}(t-t_0)}$$

$$\times [\sin \omega_{mn}(t-t_0)U(t-t_0)]e^{-a_{pq}(t'-t_0')}[\sin \omega_{pq}(t'-t_0')U(t'-t_0')]$$

$$\times \sum_{n=1}^{4} A_n K_n \int_0^a dx_0 \int_0^b dy_0 \int_0^a dx_0' \int_0^b dy_0' \frac{\phi_{mn}(x_0,y_0)\phi_{pq}(x_0',y_0')e^{-|x_0-x_0'|/\alpha_1\delta} e^{-|y_0-y_0'|/\alpha_2\delta}}{K_n^2 + \left(\frac{U_e}{\delta U_c}\right)^2 [(x_0-x_0')-U_c(t_0-t_0')]^2} \Bigg\} \quad . \qquad (24)$$

It is convenient to change the coordinates in time domain, following Maestrello (1967, page 445)

$$\tau_0' = t_0 + t_0'$$
$$\tau_0 = t_0 - t_0'$$

and replacing $t - t'$ by τ

after long manipulation Eq. (24) reduces to

$$\overline{Y(x,y,t)Y^*(x',y',t')} = \frac{\overline{p^2}g^2}{4M^2} \sum_{m,n}\sum_{p,q} \frac{\phi_{mn}(x,y)\phi_{pq}(x',y')}{\omega_{mn}\omega_{pq}\left\{\left[\left(\frac{a_{mn}+a_{pq}}{2}\right)^2 + \left(\frac{\omega_{mn}}{2}\right)^2 + \left(\frac{\omega_{pq}}{2}\right)^2\right]^2 - \frac{\omega_{mn}^2\omega_{pq}^2}{4}\right\}}$$

$$\times \sum_{n=1}^{4} A_n K_n \int_0^{\infty} dx \left\{ e^{-a_{mn}x} f(\tau - x) g_1(x) + e^{-a_{pq}x} f(\tau + x) g_2(x) \right\} \tag{25}$$

where

$$f(\tau - x) = \int_0^a dx_0 \int_0^b dy_0 \int_0^a dx_0' \int_0^b dy_0' \frac{\phi_{mn}(x_0, y_0) \phi_{pq}(x_0' y_0') e^{-|x_0 - x_0'|/\alpha_1 \delta} e^{-|y_0 - y_0'|/\alpha_2 \delta}}{K_n^2 + \left(\frac{U_e}{\delta U_c}\right)^2 [(x_0 - x_0') - U_c(\tau - x)]^2}$$

$$f(\tau + x) = \int_0^a dx_0 \int_0^b dy_0 \int_0^a dx_0' \int_0^b dy_0' \frac{\phi_{mn}(x_0, y_0) \phi_{pq}(x_0', y_0') e^{-|x_0 - x_0'|/\alpha_1} e^{-|y_0 - y_0|/\alpha_2}}{K_n^2 + \left(\frac{U_e}{\delta U_c}\right)^2 [(x_0 - x_0') - U_c(\tau + x)]^2}$$

$$g_1(x) = \omega_{mn} \omega_{pq} \left(\frac{a_{mn} + a_{pq}}{2}\right) \cos \omega_{mn} x + \omega_{pq} \left[\left(\frac{a_{mn} + a_{pq}}{2}\right)^2 - \left(\frac{\omega_{mn}}{2}\right)^2 - \left(\frac{\omega_{pq}}{2}\right)^2 \right] \sin \omega_{mn} x$$

$$g_2(x) = \omega_{mn} \omega_{pq} \left(\frac{a_{mn} + a_{pq}}{2}\right) \cos \omega_{mn} x + \omega_{mn} \left[\left(\frac{a_{mn} + a_{pq}}{2}\right)^2 + \left(\frac{\omega_{mn}}{2}\right)^2 - \left(\frac{\omega_{pq}}{2}\right)^2 \right] \sin \omega_{pq} x$$

The cross spectral density is obtained

$$\overline{Y(x,y;x',y';\omega)} = \int_{-\infty}^{\infty} Y(x,y,t)Y^*(x',y',t')e^{-i\omega\tau}d\tau$$

Let's also substitute for $\overline{x_0} = \frac{m\pi x_0}{a}$ $\overline{x_0'} = \frac{p\pi x_0'}{a}$

$$\overline{y_0} = \frac{n\pi y_0}{b} \quad \overline{y_0'} = \frac{q\pi y_0'}{b}$$

Therefore after transformation, substitution and integration with respect to x, Eq. (24) is reduced to:

$$\overline{Y(x,y;x',y';\omega)} = \frac{p(\omega)a^2b^2g^2}{M^2\pi^3} \sum_{m,n}\sum_{p,q} \frac{\phi_{m,n}(x,y)\phi_{pq}(x',y')f'(\omega)}{(mnpq)\left\{\left[\left(\frac{a_{mn}+a_{pq}}{2}\right)^2 + \left(\frac{\omega_{mn}}{2}\right)^2 + \left(\frac{\omega_{pq}}{2}\right)^2\right]^2 - \frac{\omega_{mn}^2\omega_{pq}^2}{4}\right\}}$$

$$\times \left[\frac{(a_{mn}+i\omega)\left[\left(\frac{a_{mn}+a_{pq}}{2}\right)\right] + \left\{\left(\frac{a_{mn}+a_{pq}}{2}\right)^2 - \left[\left(\frac{\omega_{mn}}{2}\right)^2 - \left(\frac{\omega_{pq}}{2}\right)^2\right]\right\}}{(a_{mn}+i\omega)^2 + \omega_{mn}^2} \right.$$

$$\left. + \frac{(a_{pq}-i\omega)\left[\left(\frac{a_{mn}+a_{pq}}{2}\right)\right] + \left[\left(\frac{a_{mn}+a_{pq}}{2}\right)^2 + \left(\frac{\omega_{mn}}{2}\right)^2 - \left(\frac{\omega_{pq}}{2}\right)^2\right]}{(a_{pq}-i\omega)^2 + \omega_{pq}^2} \right] \qquad (26)$$

where

$$f'(\omega) = \int_0^{m\pi} d\bar{x}_0 \int_0^{n\pi} d\bar{y}_0 \int_0^{p\pi} d\bar{x}_0' \int_0^{q\pi} d\bar{y}_0' \phi_{mn}\left(\frac{a\bar{x}_0}{m\pi}, \frac{b\bar{y}_0}{n\pi}\right) \phi_{pq}\left(\frac{a\bar{x}_0'}{p\pi}, \frac{b\bar{y}_0'}{q\pi}\right)$$

$$\times e^{-\frac{b}{\alpha_2 \pi}\left|\frac{\bar{y}_0}{n} - \frac{\bar{y}_0'}{q}\right|} e^{-\frac{a}{\pi\alpha_1}\left|\frac{\bar{x}_0}{m} - \frac{\bar{x}_0'}{p}\right|} e^{-\frac{i\omega}{U_c}\left[\frac{a}{\pi}\left(\frac{\bar{x}_0}{m} - \frac{\bar{x}_0'}{p}\right)\right]}$$

for the case where the panel modes are well separated, one neglects modal coupling, Eq. (26) then reduces for $m = p$; $n = q$ to:

$$\overline{Y(x,y;x',y';\omega)} = \frac{4P(\omega)a^2b^2g^2}{M^2\pi^3} \sum_{mn} \frac{\phi_{mn}(x,y)\phi_{mn}(x',y')}{m^2n^2\left[\left(a_{mn}^2+\omega_{mn}^2+\omega^2\right)^2 - 4\omega_{mn}^2\omega^2\right]}$$

$$\times \int_0^{m\pi} d\bar{x}_0 \int_0^{n\pi} d\bar{y}_0 \int_0^{m\pi} d\bar{x}_0' \int_0^{n\pi} d\bar{y}_0' \phi_{mn}\left(\frac{a\bar{x}_0}{m\pi}, \frac{b\bar{y}_0}{n\pi}\right) \phi_{mn}\left(\frac{a\bar{x}_0'}{m\pi}, \frac{b\bar{y}_0'}{n\pi}\right) e^{-\frac{b}{n\pi\alpha_2}\left|\bar{y}_0 - \bar{y}_0'\right|} e^{-\frac{a}{m\pi\alpha_1}\left|\bar{x}_0 - \bar{y}_0'\right|}$$

$$\times e^{-\frac{i\omega}{U_c}\left[\frac{a}{m\pi}(\bar{x}_0 - \bar{x}_0')\right]} \qquad (27)$$

In computing the spectral density one has to specify the eigenfunction $\phi(x,y)$ and $\phi(\frac{ax_0}{m\pi}, \frac{by_0}{n\pi})$. Only for a simply supported boundary the exact solution is known, and opportunity has been taken of this solution to carry out the closed form solution for the response cross spectral density (appendix b). The simply supported boundaries are not physically realistic; one has to consider spring type edges conditioned to allow rotation and translation constrained.

Yang (1950) used the Ritz method to find the dynamic characteristics of rectangular plates with continuum spring boundary conditions. More recently this method has been brought up by Izzo, Baylor, and Robideaus (1960). The present analysis does not restrict the usage of any particular method (i.e., Ritz, Galerkin or Rayleigh) for example in the case of the present experiment the panel boundaries are clamped; Warburton's (1954) approximation is used in the computation.

The acoustic power radiated by the panel is obtained by the same procedure used to compute the acoustic power radiated by the turbulent boundary layer described in the next section. Using this result expressed in terms of the panel displacement cross spectral density $Y(\underset{\sim}{\lambda};\omega)$ rather than the pressure cross spectral density over the rigid wall $P(\underset{\sim}{\lambda};\omega)$ the radiated power spectral density is given by

$$P_r(\omega) = \frac{\omega^2 \rho}{2\pi c} \int_{s(\underset{\sim}{\lambda})} Y(\underset{\sim}{\lambda};\omega) \left| (\sin \frac{\omega|\lambda|}{c}) / \frac{\omega|\lambda|}{c} - \cos \frac{\omega|\lambda|}{c} \right| \frac{d\underset{\sim}{\lambda}}{|\underset{\sim}{\lambda}|^2} \qquad (28)$$

where $\underset{\sim}{\lambda} = \sqrt{(x-x_o')^2 - (y-y_o')^2}$.

The pressure radiating modes of the flexible panel mounted on an infinite rigid plane is in phase with panel velocity, the wave motion has supersonic phase velocity, the energy losses appear as a damping of the panel response. While the subsonic components (near the plate surface) appear as additional mass, they are of predominant lower frequency.

V. Comparison with Measurements

A good comparison is made with calculation for two panel configurations, one with 0.06 psi pressure differential enclosed in a cavity (Figs. 20, 21 and 22) and the other with 14 psi pressure differential radiating into open air (Fig. 23). The calculations are based on the analysis discussed in the previous section which does not account for the additional forcing field, the pressure induced by panel motion. However, the damping used in the calculation are those values obtained experimentally. As indicated previously, the damping is mainly acoustic and thus one can ignore the mechanical damping. The subsonic component of the velocity is out of phase with panel velocity and therefore no dissipation of energy occurs. The rise of the virtual mass due to the subsonic component is small for an air medium and it can be ignored. By making $e^{-a_{mn}(t-t_0)} = 1$ in the Green's function and taking into account the pressure induced by the panel motion the acoustic damping will be a part of the solution. This calculation procedure is a result of the present work and will soon be reported. It is expected that the new method (Maestrello, McDaid) in computing the response may not differ more than a factor of two (in the present case). In addition to the case where the plate motion alters the turbulent boundary layer a perturbation pressure similar to Kuo (1965) in study of the surface roughness has to be added.

The pressurized panel has lower displacement spectra than the unpressurized one. In fact the static loading $N_x \frac{\partial^2 Y}{\partial x^2} + N_y \frac{\partial^2 Y}{\partial y^2} + \Delta P$ is the contribution of it. The shift in frequency from the pressure of 0.06 to 14 psi is from 475 to 595 hz in the fundamental mode. This is accomplished by a change in static deflection of about 0.07 inch at the panel center, effectively increasing the stiffness of the panel.

VI. Sound Radiation from Turbulent Boundary Layer

In the previous chapter an attempt is made to link the forcing field of the turbulent wall pressure to the response field of a typical panel structure by means of a statistical method. In a similar fashion utilizing the temporal and spatial correlation of the wall pressure, separation is obtained of the acoustic mode, that is the weakest mode within the flow field, from the vorticity and entropy modes being the stronger by far.

The acoustic power predicted is obtained by imaging techniques where the properties of the far field noise are connected to the statistical properties of the boundary layer via near field pressure over the wall. Powell (1960) showed that a plane rigid surface reflects the sound radiated by an equivalent quadrupole located in the flow stream above the surface. The surface imaging pressure field is identical to measurements made of space-time correlation of the double time derivative of the Reynolds stresses and integrated over the turbulent field (Lighthill results). Where the flow is over the surface the reflection from the surface could be distorted due to the action of viscous stress; it has been argued, however, that the normal stress on the surface is negligible*. With this assumption the problem is equivalent to that of an image boundary layer in which the acoustic power radiated per unit volume of turbulence could be related to the correlation area of the pressure on the surface. Since the surface is rigid no acoustic energy can be generated but it is generated within the turbulence due to variation of the eddy strength caused by the fluctuating volume.

Laufer (1961) made the first measurements of sound radiated by a supersonic turbulent boundary layer, by means of a hot wire annemometer,

*Leehey (1968) recognized that the neglected surface integral in the evaluation of the wall pressure fluctuation gives rise to oscillatory wall shear stresses. Leehey's observation came to the author's attention after this manuscript was written, therefore the results of the implication above are not yet known.

correlating in space and time outside the boundary layer. The loss of energy from the turbulence shearing stress by acoustic radiation is very small, therefore the detection and measurement made by Laufer was quite a challenge. His results agree qualitatively with the model of the radiation field as predicted by Phillips at higher Mach numbers.

Wilson (1960) also measured the sound radiated from a subsonic boundary layer around a rotating cylinder. He placed the rotating cylinder into a reverberation room; the acoustic pressure radiated from the boundary layer was obtained after eliminating the mechanical noise of the rotating mechanism.

Ffowcs Williams and Maidanik (1965) computed the mean square radiated pressure in terms of surface pressure fluctuations using Lighthill formalization. Their results well agree with the measurements made by Laufer.

In formulating the present problem, let us recall some fundamental flow field equations. Assuming the flow is incompressible, uniform density ρ, the pressure p obeys the following relationship

$$\nabla^2 p(\underset{\sim}{x}) = - f(\underset{\sim}{x}) \tag{29}$$

the free field solution $f = 0$ at infinity is given by

$$p(\underset{\sim}{x}) = - \frac{1}{4\pi} \int_V \frac{\nabla^2 p(\underset{\sim}{y})}{|\underset{\sim}{x} - \underset{\sim}{y}|} \, d\underset{\sim}{y} \tag{30}$$

or

$$p(\underset{\sim}{x}) = \frac{1}{4\pi} \int_V \frac{f(\underset{\sim}{y})}{|\underset{\sim}{x} - \underset{\sim}{y}|} \, d\underset{\sim}{y} \tag{31}$$

the surface being infinite rigid and plane an additional boundary condition is imposed.

Then

$$P_s(\underset{\sim}{x}) = -\frac{1}{4\pi}\int_V \frac{\nabla^2 p(\underset{\sim}{y})}{|\underset{\sim}{x}-\underset{\sim}{y}|}\, d\underset{\sim}{y}$$

$$= \frac{1}{4\pi}\int_V \nabla\cdot\nabla\left(\frac{P}{|x-y|}\right) dy + \frac{1}{2\pi}\int_V \nabla\cdot\left(P\nabla\frac{1}{|x-y|}\right) d\underset{\sim}{y} \qquad (32)$$

from Gauss's theorem

$$P_s(\underset{\sim}{x}) = -\frac{1}{4\pi}\int_S \left[\frac{1}{|\underset{\sim}{x}-\underset{\sim}{y}|}\frac{\partial P}{\partial n} - P\frac{\partial}{\partial n}\left(\frac{1}{|\underset{\sim}{x}-\underset{\sim}{y}|}\right)\right] d\underset{\sim}{y} \qquad (33)$$

The general solution is obtained by adding Equations (31 and 33)

$$P(\underset{\sim}{x}) = \frac{1}{4\pi}\int_V \frac{f(\underset{\sim}{y})}{|\underset{\sim}{x}-\underset{\sim}{y}|}\, d\underset{\sim}{y} - \frac{1}{4\pi}\int_S \left[\frac{1}{|\underset{\sim}{x}-\underset{\sim}{y}|}\frac{\partial P}{\partial n} - P\frac{\partial}{\partial n}\left(\frac{1}{|\underset{\sim}{x}-\underset{\sim}{y}|}\right)\right] d\underset{\sim}{y} \qquad (34)$$

is the solution of Poisson's equation for the case of a rigid boundary. If one takes the pressure P at the retarded time $|x-y|/c$ where c is the propagation velocity, the abcve equation becomes the solution of the inhomogeneous wave equation. Evaluating $\left[\frac{\partial P}{\partial n}\right]^x$ one obtains:

$$\left[\frac{\partial P}{\partial n}\right]^x = \left[\frac{\partial P}{\partial n} + \frac{\partial P}{\partial t}\,\frac{\partial t}{\partial(|\underset{\sim}{x}-\underset{\sim}{y}|)}\,\frac{\partial(|\underset{\sim}{x}-\underset{\sim}{y}|)}{\partial n}\right]_{t=-\frac{|\underset{\sim}{x}-\underset{\sim}{y}|}{c}}$$

$$= \frac{\partial P}{\partial n}\left(\underset{\sim}{y},\ t-\frac{|\underset{\sim}{x}-\underset{\sim}{y}|}{c}\right) - \frac{1}{c}\,\frac{\partial(|\underset{\sim}{x}-\underset{\sim}{y}|)}{\partial n}\,\frac{\partial P}{\partial t}\left(\underset{\sim}{y},t-\frac{(|\underset{\sim}{x}-\underset{\sim}{y}|)}{c}\right) \qquad (35)$$

Substituting into (34)

$$P(\underset{\sim}{x},t) = \frac{1}{4\pi}\int_V f\left(\underset{\sim}{y},t-\frac{|\underset{\sim}{x}-\underset{\sim}{y}|}{c}\right)\frac{d\underset{\sim}{x}}{|\underset{\sim}{x}-\underset{\sim}{y}|} + \frac{1}{4\pi}\int_S \left\{\frac{1}{|\underset{\sim}{x}-\underset{\sim}{y}|}\frac{\partial P}{\partial n}\left(\underset{\sim}{y},\ t-\frac{|\underset{\sim}{x}-\underset{\sim}{y}|}{c}\right)\right.$$

$$\left. - \frac{1}{c|\underset{\sim}{x}-\underset{\sim}{y}|}\left[\frac{\partial(|\underset{\sim}{x}-\underset{\sim}{y}|)}{\partial n}\right]\frac{\partial P}{\partial t}\left(\underset{\sim}{y},\ t-\frac{|\underset{\sim}{x}-\underset{\sim}{y}|}{c}\right) - P\left(\underset{\sim}{y},t-\frac{|\underset{\sim}{x}-\underset{\sim}{y}|}{c}\right)\frac{\partial}{\partial n}\left(\frac{1}{|\underset{\sim}{x}-\underset{\sim}{y}|}\right)\right\} dS \qquad (36)$$

The above equation is the well-known Kirchhoff solution. The volume integral expresses the contribution of sound from the turbulence, while the surface integral is the contribution of the sound upon the surface. By imaging, the two integrals are identical. Three terms appear in the surface integral, the first gives the contribution of the usual pressure on the surface, the second describes the radiated pressure from the apparent sources, and the third term describes the near field pressure which decays $1/r$ faster than the radiated pressure $r \equiv |\underset{\sim}{x} - \underset{\sim}{y}|$.

Then, the radiated pressure

$$P(\underset{\sim}{x}, t) = -\frac{1}{4\pi c}\int_S \frac{\partial r}{\partial n}\frac{\partial P}{\partial t}\left(y, t - \frac{r}{c}\right)\frac{dS}{r}$$

$$= \frac{\cos\theta}{4\pi c}\int_S \frac{\partial P}{\partial t}\left(y, t - \frac{r}{c}\right)\frac{dS}{r} \qquad (37)$$

The corresponding pressure correlation

$$R(\underset{\sim}{x}, \underset{\sim}{y}, t) = \frac{\cos^2\theta}{16\pi^2 c^2 r^2}\int_{S(\underset{\sim}{\lambda})}\int_{S(\underset{\sim}{y})} \frac{\partial P}{\partial t}\left(\underset{\sim}{y} + \underset{\sim}{\lambda}, t - \frac{r + \lambda\sin\theta\cos\phi}{c}\right)$$

$$\times \frac{\partial P}{\partial t}\left(\underset{\sim}{y}, t - \frac{r}{c}\right) d\underset{\sim}{y}\, d\underset{\sim}{\lambda} \qquad (38)$$

where $r' = r + \underset{\sim}{\lambda}\ \sin\theta\cos\phi$

$$R(\underset{\sim}{x}, \underset{\sim}{y}; \tau) = \frac{\cos^2\theta}{16\pi^2 r^2 c^2}\int_{S(\underset{\sim}{\lambda})}\int_{S(\underset{\sim}{y})} \frac{\partial^2}{\partial\tau^2} P\left(\underset{\sim}{\lambda}, \tau = \frac{\lambda\sin\theta\cos\phi}{c}\right) d\underset{\sim}{\lambda}\, d\underset{\sim}{y} \qquad (39)$$

From the theory of Fourier transforms one obtains

$$R(\underset{\sim}{x},\underset{\sim}{y};\omega)= \frac{\omega^2 \cos^2\theta}{16\pi^2 r^2 c^2}\int_{S(\underset{\sim}{\lambda})}\int_{S(\underset{\sim}{y})} P(\underset{\sim}{\lambda};\omega)\, e^{i\omega \frac{\underset{\sim}{\lambda}}{c} \sin\theta \cos\phi}\, d\underset{\sim}{\lambda}\, d\underset{\sim}{y} \qquad (40)$$

The power spectral density per unit area of the acoustic pressure field is obtained by

$$\frac{\partial}{\partial \underset{\sim}{y}} P(\underset{\sim}{y},\omega) = \frac{1}{\rho c}\int \frac{\partial}{\partial \underset{\sim}{y}} R(\underset{\sim}{x},\underset{\sim}{y};\omega) = \frac{1}{\rho c}\int_{\theta=0}^{\pi/2}\int_{\phi=0}^{2\pi} r^2 d\theta\, \sin\theta d\phi\, \frac{\partial}{\partial \underset{\sim}{y}} R(\underset{\sim}{x},\underset{\sim}{y};\omega)$$

$$= \frac{\omega^2}{16\rho\pi^2 c^3}\int_{\theta=0}^{\pi/2}\int_{\phi=0}^{2\pi} \cos^2\theta\, \sin\theta d\theta d\phi \int_{S(\lambda)} P(\lambda;\omega) e^{i\omega \frac{\lambda}{c} \sin\theta \cos\phi}\, d\underset{\sim}{\lambda}$$

$$= \frac{1}{8\pi\rho c}\int_{S(\underset{\sim}{\lambda})} P(\underset{\sim}{\lambda};\omega)\left\{\left(\sin\frac{\omega|\lambda|}{c}\right)\Big/\frac{\omega|\lambda|}{c} - \cos\frac{\omega|\lambda|}{c}\right\}\frac{d\underset{\sim}{\lambda}}{|\underset{\sim}{\lambda}|^2} \qquad (41)$$

where $P(\underset{\sim}{\lambda};\omega)$ is the power spectral density of the pressure field.

The integrand behavior is such that as $\omega|\lambda|/c$ tends to zero the term $\{\quad\}\frac{1}{|\lambda|^2} \approx \omega^2/c^2$, meaning the radiated spectrum will peak higher than the near field pressure, a result consistent with Lyamshev (1961).

For turbulent boundary layer a model of $P(\underset{\sim}{\lambda};\omega)$ is given by

$$P(\xi,\eta;\omega) = P(\omega) e^{-|\xi|/\alpha_1} e^{-|\eta|\alpha_2} \cos\frac{\omega\xi}{U_c}$$

where

$$P(\omega) = \frac{\overline{P^2}\delta}{U_e}\sum A_n e^{-K_n \omega\delta/U_e}$$

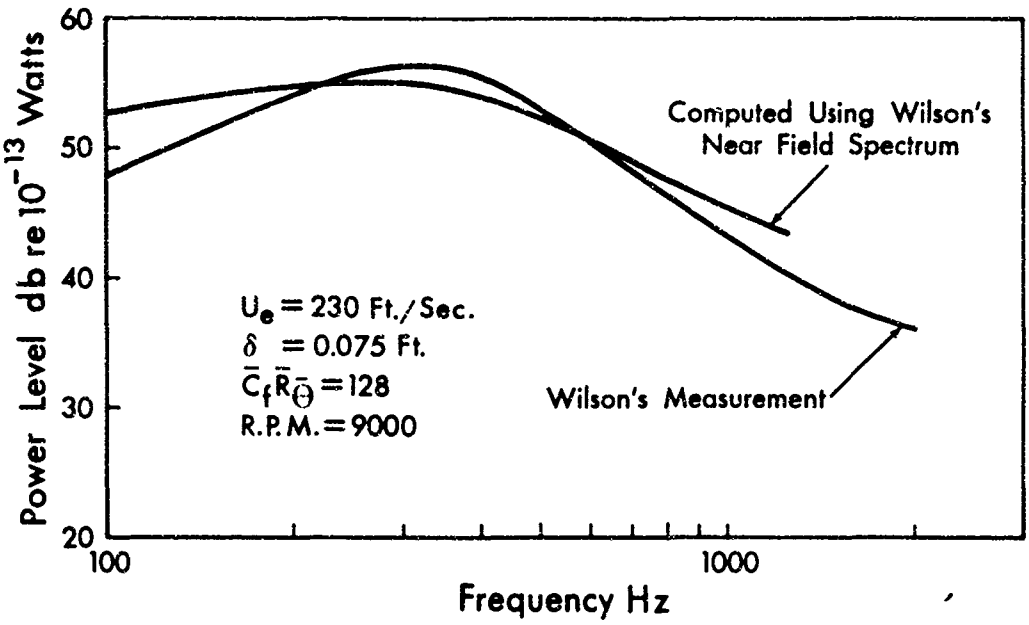

Fig. 27. Acoustic power level from turbulent boundary layer over a rotating cylinder.

and

$$\lambda = \sqrt{\xi^2 + \eta^2} \ .$$

Wilson's experiment is used for comparison with the present analysis Fig. (27). In order to compute the acoustic power radiated by the turbulent boundary layer on a rotating cylinder one needs to evaluate the cross spectral density $P(\underset{\sim}{\lambda},\omega)$. The model of the turbulent boundary over a flat plate is adopted for $P(\underset{\sim}{\lambda},\omega)$ and Wilson's near field pressure spectrum is used since at lower frequencies the near field power spectrum differs from that over a flat plate. The resulting comparison is satisfactory.

For subsonic flow the cross spectral density $P(\underset{\sim}{\lambda},\omega)$ is proportional to

$$M_e^2 \rho^2 U_e^3 \delta$$

and the acoustic power is proportional to

$$\rho U_e^3 M_e^5 \delta$$

while for Mach wave radiation the cross spectral density $P(\underset{\sim}{\lambda},\omega)$ is proportional to

$$\rho^2 U_e^3 \delta$$

and the acoustic power is proportional to

$$\rho U_e^3 \delta^2 .$$

In attempting to compute Laufer's Mach wave radiation, a difficulty is encountered since he measured the intensity at a point

while this analysis obtains the power per unit area. In the comparison one would have to account for the Doppler shift $\left(\frac{M_e}{M_c} - 1\right)$ since Laufer's measurements are in a moving stream along the Mach line. The condition for Mach wave radiation is such that $|Mc - M| > 1$. This implies that the comparison has to be made for $M_e > 3.5$.

Phillips has shown that radiated sound arises from eddy Mach waves which are generated by some wave numbers of the turbulence in those layers for which the difference between the mean velocity of the fluid outside and the local eddy velocity is greater than the speed of sound. This mechanism appears consistent with the present results.

APPENDIX A

Prove that the displacement cross correlation is even in τ

$$\overline{Y(x,y,t)\,Y(x',y',t')}$$

$$= \frac{abp^2}{2\pi^2 M^2} \sum_{m\ n} \frac{\phi_{mn}(x,y)\,\phi_{mn}(x',y')}{m\ n\ \omega_{mn}\left(a^2_{mn} + \omega^2_{mn}\right)} I_{mn}$$

where

$$I_{mn} = \int_{-m\pi}^{m\pi} f(z) \left[\int_{o}^{n\pi} f(y) \left[\int_{o}^{\infty} g(x) \sum_{n=1}^{4} \left\{ \frac{A_n K_n e^{-\left|\frac{az}{\pi\alpha_1}\right|}}{K^2_n + \left(\frac{U_e}{\delta U_c}\right)^2 \left[\left(\left[\frac{az}{m\pi} - U_c\tau \right] + U_c x \right)^2 + \left(\frac{by}{n\pi}\right)^2 \right]} \right.\right.\right.$$

$$\left.\left.\left. + \frac{A_n K_n e^{-\left|\frac{az}{m\pi\alpha_1}\right|}}{K^2_n + \left(\frac{U_e}{\delta U_c}\right)^2 \left[\left(\left[\frac{az}{m\pi} - U_c\tau \right] - U_c x \right)^2 + \left(\frac{by}{n\pi}\right)^2 \right]} \right\} dx \right] dy \right] dz$$

Let us define

$$F_1(\tau) = \int_{-m\pi}^{m\pi} f(z) \int_0^{\infty} g(x) \left\{ \frac{1}{G\left(\left[\frac{az}{m\pi} - U_c(\tau - x)\right]^2\right)} + \frac{1}{G\left(\left[\frac{az}{m\pi} - U_c(\tau + x)\right]^2\right)} \right\} dx\, dz$$

$$= \int_{-m\pi}^{m\pi} f(z) \int_0^{\infty} g(|x|) \frac{1}{G\left(\left[\frac{az}{m\pi} - U_c(\tau - x)\right]^2\right)} dx\, dz$$

Set $X = \tau - x$

$$F_1(\tau) = \int_{-m\pi}^{m\pi} f(z) \int_{-\infty}^{\infty} g(|\tau - x|) \frac{1}{G\left(\left[\frac{az}{m\pi} - U_c X\right]^2\right)} dX\, dz$$

then

$$F_1(-\tau) = \int_{-m\pi}^{m\pi} f(z) \int_{-\infty}^{\infty} g(|\tau - X|) \frac{1}{G\left(\left[\frac{az}{m\pi} - U_c X\right]^2\right)} dX\, dz$$

Set $x = -X$

$$F_1(-\tau) = \int_{-m\pi}^{m\pi} f(z) \int_{-\infty}^{\infty} g(|\tau - x|) \frac{1}{G\left(\left[\frac{az}{m\pi} + U_c x\right]^2\right)} dx\, dz$$

Set $Z = -z$

$$F_1(-\tau) = \int_{-m\pi}^{m\pi} f(-Z) \int_{-\infty}^{\infty} g\left(|\tau - x|\right) \frac{1}{G\left(\left[-\frac{az}{m\pi} + U_c x\right]^2\right)} \, dx \, dZ$$

$$= \int_{-m\pi}^{m\pi} f(Z) \int_{-\infty}^{\infty} g\left(|\tau - x|\right) \frac{1}{G\left(\left[\frac{az}{m\pi} - U_c x\right]^2\right)} \, dx \, dZ$$

$$= F_1(\tau)$$

APPENDIX B

The following is the closed form solution of the panel deflection cross power spectral density (Eq. 24) for simply supported boundaries without cross modal coupling. From Maestrello (1967) one can obtain the following cross correlation of the panel displacement.

$$\overline{Y(x,y,t)Y(x',y',t')} = \frac{abp^{\overline{2}}}{2\pi^2 M^2} \sum_{m,n} \frac{\phi_{mn}(x,y)\,\phi_{mn}(x',y')}{m\,n\,\omega_{mn}\left(a^2_{mn} + \omega^2_{mn}\right)} I_{mn} \tag{1B}$$

where

$$I_{mn} = \int_{-m\pi}^{m\pi} f(z)\left[\int_0^{n\pi} f(y)\left[\int_0^{\infty} g(x)\sum_{n=1}^{4}\left\{ \frac{A_n K_n}{K^2_n + \left(\frac{\delta U_e}{U_c}\right)^2\left[\left(\left[\frac{az}{m\pi} - U_c\tau\right] + U_c x\right)^2 + \left(\frac{by}{n\pi}\right)^2\right]} \right.\right.\right.$$

$$\left.\left.\left. + \frac{A_n K_n}{K^2_n + \left(\frac{\delta U_e}{U_c}\right)^2\left[\left(\left[\frac{az}{m\pi} - U_c\tau\right] - U_c x\right)^2 + \left(\frac{by}{n\pi}\right)^2\right]} \right\} dx\right] dy\right] dz$$

and $$f(z) = \frac{\cos z + \frac{1}{m\pi}(-|z|\cos z + \sin|z|)}{e^{|(az/m\pi\alpha_1|}}$$

$$f(y) = \frac{\cos y + \frac{1}{n\pi}(\sin y - y\cos y)}{e^{|by/n\pi\alpha_2|}}$$

$$g(x) = e^{-a_m x}\left[\sin \omega_{mn} x + \frac{\omega_{mn}}{a_{mn}} \cos \omega_{mn} x\right]$$

$$\phi_{mn}(x,y) = \frac{2}{(ab)^{\frac{1}{2}}} \sin \frac{m\pi x}{a} \sin \frac{n\pi y}{b}$$

I_{mn} is an even function of τ and $\overline{Y(x,y,t)\ Y\ (x',y',t')}$ is also even as shown in (appendix a); one can obtain the auto correlation by setting $x = x'$ and $y = y'$ in (1B). The displacement cross spectral density is obtained:

$$P\left[\overline{Y(x,y,t)Y\ (x',y',t');\ \omega}\right] = \frac{1}{2\pi} \int_{-\infty}^{\infty} \overline{Y(x,y,t)Y\ (x',y',t')}\ e^{i\omega\tau} d\tau \qquad (2B)$$

From (2B) and integrating with respect to x one obtains:

$$P\left[\overline{Y(x,y,t)Y\ (x',y',t');\omega}\right] = \frac{ab\ P(\omega) g^2}{4\pi^2\ M^2} \sum_{m,n} \frac{\phi_{mn}(x,y)\phi_{mn}(x',y')}{mn\ \omega_{mn}\left(a^2_{mn} + \omega^2_{mn}\right)} \times$$

$$\left(\int_0^{m\pi} dz \int_0^{n\pi} dy \int_0^{\infty} dx\ f(z)f(y)g(x)\right) e^{-i\omega az/m\pi U_c} \cos \omega x \qquad (3B)$$

Simplify the above equation by integrating out the g(x) and f(z) integrals;

The g(x) integral reduces to:

$$\int_0^\infty dx\ e^{-a_{mn}x}\left[\sin\left(\omega_{mn}x\right)+\frac{\omega_{mn}}{a_{mn}}\cos\left(\omega_{mn}x\right)\right]$$

$$=\frac{2\omega_{mn}\left(a_{mn}^2+\omega_{mn}^2\right)}{\left(a_{mn}^2+\omega_{mn}^2+\omega^2\right)^2-4\,\omega_{mn}^2\,\omega^2}$$

and the z integral reduces to:

$$\frac{1}{2}\int_0^{m\pi} dz\left[\cos\left(1+\frac{\omega a}{m\pi U_c}\right)z+\cos\left(1-\frac{\omega a}{m\pi U_c}\right)z\right]e^{-|az/m\pi\alpha_1|}$$

$$-\frac{1}{2}\,\frac{1}{n\pi}\int_0^{m\pi'} dz\ |z|\left[\cos\left(1+\frac{\omega a}{m\pi U_c}\right)z+\cos\left(1-\frac{\omega a}{m\pi U_c}\right)z\right]e^{-|az/m\pi\alpha_1|}$$

$$+\frac{1}{m\pi}\int_0^{m\pi} dz\ \sin|z|\ \cos\left(\frac{\omega az}{m\pi U_c}\right)e^{-|az/m\pi\alpha_1|}$$

$$=\left[I_1+I_2+I_3+I_4+I_5\right]$$

where

$$I_1 = \left[\frac{e^{-a/\alpha_1} m\pi\alpha_1}{a^2 + \left(m\pi\alpha_1 + \omega a\theta\right)^2}\right]\left[-a\cos\left(\frac{m\pi U_c + \omega a}{U_c}\right) + \left(m\pi\alpha_1 + \omega a\theta\right)\sin\left(\frac{m\pi U_c + \omega a}{U_c}\right) + a\right]$$

$$I_2 = \left[\frac{e^{-a/\alpha_1} m\pi\alpha_1}{a^2 - \left(m\pi\alpha_1 - \omega a\theta\right)^2}\right]\left[-a\cos\left(\frac{m\pi U_c - \omega a}{U_c}\right) + \left(m\pi\alpha_1 - \omega a\theta\right)\sin\left(\frac{m\pi U_c - \omega a}{U_c}\right) + a\right]$$

$$I_3 = \frac{e^{-a/\alpha_1} m^2\pi^2\alpha_1^2}{a^2 + \left(m\pi\alpha_1 + \omega a\theta\right)^2}\left[\left\{-\frac{a}{\alpha_1} - \frac{a^2 - \left(m\pi\alpha_1 + \omega a\theta\right)^2}{a^2 + \left(m\pi\alpha_1 + \omega a\theta\right)^2}\right\}\cos\left(\frac{m\pi U_c + \omega a}{U_c}\right) + \right.$$

$$\left\{\left(\frac{m\pi U_c + \omega a}{U_c} - \frac{(-2a)\left(m\pi\alpha_1 + \omega a\theta\right)\left(m\pi U_c\theta\right)}{a^2 + \left(m\pi\alpha_1 + \omega a\theta\right)^2}\right\}\sin\left(\frac{m\pi U_c + \omega a}{U_c}\right) +$$

$$\left.\left(\frac{a^2 - \left(m\pi\alpha_1 + \omega a\theta\right)^2}{a^2 + \left(m\pi\alpha_1 + \omega a\theta\right)^2}\right)\right] e^{-a/\alpha_1}$$

$$I_4 = \frac{e^{-a/\alpha_1} m^2\pi^2\alpha_1^2}{a^2 + \left(m\pi\alpha_1 - \omega a\theta\right)^2}\left[\left\{-\frac{a}{\alpha_1} - \frac{a^2 - \left(m\pi\alpha_1 - \omega a\theta\right)^2}{a^2 + \left(m\pi\alpha_1 - \omega a\theta\right)^2}\right\}\cos\left(\frac{m\pi U_c - \omega a}{U_c}\right) + \right.$$

$$\left\{\left(\frac{m\pi U_c - \omega a}{U_c}\right) - \frac{(-2a)\left(m\pi\alpha_1 - \omega a\theta\right)\left(m\pi\alpha_1\right)}{a^2 + \left(m\pi\alpha_1 - \omega a\theta\right)^2}\right\}\sin\left(\frac{m\pi U_c - \omega a}{U_c}\right) +$$

$$\left.\left(\frac{a^2 - \left(m\pi\alpha_1 - \omega a\theta\right)^2}{a^2 + \left(m\pi\alpha_1 - \omega a\theta\right)^2}\right)\right] e^{-a/\alpha_1}$$

$$I_5 = \frac{e^{-a/\alpha_1} m^2\pi^2\alpha_1^2}{2\left[a^2+\left(m\pi\alpha_1+\omega a\theta\right)^2\right]}\left[\frac{-a}{m\pi\alpha_1}\sin\left(\frac{m\pi U_c+\omega a}{U_c}\right) -\right.$$

$$\left.\frac{m\pi\alpha_1+\omega a}{\pi\alpha_1}\right)\cos\left(\frac{m\pi U_c+\omega a}{U_c}\right)\left(\frac{m\pi\alpha_1+\omega a\theta}{m\pi\alpha_1}\right)\Bigg] -$$

$$\frac{e^{-a/\alpha_1} m^2\pi^2\alpha_1^2}{2\left[a^2+\left(m\pi\alpha_1-\omega a\theta\right)^2\right]}\left[\frac{-a}{m\pi\alpha_1}\sin\left(\frac{m\pi U_c-\omega a}{U_c}\right)-\right.$$

$$\left.\left(\frac{m\pi\alpha_1-\omega a\theta}{m\pi\alpha_1}\right)\cos\left(\frac{m\pi U_c-\omega a}{U_c}\right)+\left(\frac{m\pi\alpha_1-\omega a\theta}{m\pi\alpha_1}\right)\right]$$

Finally the f(y) integral reduces to:

$$\int_0^{n\pi} dy\, f(y) = \int_0^{n\pi} dy\, e^{-\frac{by}{n\pi\alpha_2}} \cos y + \frac{1}{n\pi}\int_0^{n\pi} e^{-\frac{by}{n\pi\alpha_2}} \sin y -$$

$$\frac{1}{n\pi}\cdot\int_0^{n\pi} dy\, y\, e^{-\frac{by}{n\pi\alpha_2}} \cos y = I_6$$

$$\text{where } I_6 = \frac{e^{-b/\alpha_2}\cos n\pi}{n\pi\left[\left(\frac{b}{n\pi\alpha_2}\right)^2 + 1\right]}\left[\frac{\left(\frac{b}{\alpha_2}\right)^2 - n^2\pi^2}{\left(\frac{b}{\alpha_2}\right)^2 + n^2\pi^2} - 1\right]$$

$$+ \frac{e^{-b/\alpha_2}\sin n\pi}{n\pi\left[\left(\frac{b}{n\pi\alpha_2}\right)^2 + 1\right]}\left[\frac{\frac{2bn\pi}{\alpha_2}}{\left(\frac{b}{\alpha_2}\right)^2 + n^2\pi^2} - \frac{\frac{b}{\alpha_2}}{n\pi}\right]$$

$$+ \frac{1}{n\pi\left[\left(\frac{b}{\alpha_2 \pi n}\right)^2 + 1\right]}\left[\frac{b}{\alpha_2} - \frac{\left(\frac{b}{\alpha_2}\right)^2 - n^2\pi^2}{\left(\frac{b}{\alpha_2}\right)^2 + n^2\pi^2} + 1\right]$$

The cross spectral density is finally reduced to:

$$P[Y(x,y,t)Y(x',y',t');\omega] = \frac{ab\varepsilon^2 P(\omega)}{\pi^2 M^2} \times$$

$$\sum_{m,n} \frac{\phi_{mn}(x,y)\phi_{mn}(x',y')}{mn[a_{mn}^2 + \omega_{mn}^2 + \omega^2] - 4\omega_{mn}^2\omega^2} (I_1+I_2+I_3+I_4+I_5)I_6$$

ACKNOWLEDGMENT

The author would like to express his gratitude to Mrs. Francita Gasche and Mr. S. D. Hansen for the development of computer programs, and E. M. Harris, C. McDaid and R. Skoog for their technical assistance.

REFERENCES

Baronti, P. O. and Libby, P. A. (1966), Velocity Profiles in Turbulent Compressible Boundary Layers, *AIAA Journal*, Vol. 4, No. 2.

Bradshaw, P. (1965), "Inactive" Motion and Pressure Fluctuations in Turbulent Boundary Layers, Aero. Rep. 1172.

Bull, M. K. (1967), Wall-Pressure Fluctuations Associated with Subsonic Turbulent Boundary Layer Flow, *J. Fluid Mech.*, Vol. 28, Part 4.

Coles, D. (1963), The Turbulent Boundary Layer in a Compressible Fluid, *Physics of Fluids*, Vol. 7, No. 9.

Corcos, G. M. (1962), Pressure Fluctuations in Shear Flow, University of California Report Series 183/2.

Corcos, G. M. (1967), Resolution of the Turbulent Pressures at the Wall of a Boundary Layer, *Journal Sound Vibration*, Vol. 6, No. 1.

Crocker, M. J. and White, R. W. (1966), Response of the Lockheed L-200 Supersonic Transport Fuselage to Turbulence and Reverberant Noise.

Doak, P. E. (1960), Acoustic Radiation from a Turbulent Fluid Containing Foreign Body, *Proc. Royal Soc.* A-254.

Donaldson, C. du P. (1952), On the Form of the Turbulent Skin Friction Law and Its Extension to Compressible Flows, NACA TN 2692.

Dowell, E. H. and Voss, H. M. (1963), The Effect of a Cavity on Panel Vibration, *AIAA Journal*, Vol. 1, 476.

Dowell, E. H. (1966), Nonlinear Oscillations of a Fluttering Plate, *AIAA Journal*, Vol. 4.

Dowell, E. H. (1967), Generalized Aerodynamic Forces on a Flexible Plate Undergoing Transient Motion, *Quart. Appl. Math.*, Vol. 24.

Dyer, I. (1958), Sound Radiation Into a Closed Space from Boundary Layer Turbulence, Bolt, Beranek, and Newman, Inc., Report No. 602.

Favre, A. J., Gaviglio, J. and Dumas, R. (1967), Structure of Velocity Space-Time Correlations in a Boundary Layer, *The Physics of Fluids Suppl.*, S138-S152.

Ffowcs Williams, J. E. and Lyon, R. H. (1963), The Sound Radiated from Turbulent Flows Near Flexible Boundaries, BBN Report No. 1054.

Ffowcs Williams, J. E. (1964), Surface Pressure Fluctuations Induced by Boundary Layer Flow at Finite Mach Number, *J. Fluid Mech.*, Vol. 22, Part 3.

Ffowcs Williams, J. E. and Maidanik (1965), The Mach Wave Field Radiated by Supersonic Turbulent Shear Flows, *J. Fluid Mech.*, Vol. 21, Part 4.

Ffowcs Williams, J. E. (1966), The Influence of Simple Supports on the Radiation from Turbulent Flow Near a Plane Compliant Surface, *J. Fluid Mech.*, Vol. 26, Part 4.

Hodgson, T. H. (1962), Pressure Fluctuations in Shear Flow Turbulence, College of Aeronautics Note No. 129.

Izzo, A. J., Baylor, J. L. and Robideau, R. F. (1960), Sound Radiated from Turbulence-Excited Finite Plates with Arbitrary Boundary Conditions, General Dynamics Electric Boat Division, Report No. U411-66-051.

Jacobs, L. D. and Lagerquist, D. R. (1967), A Finite Element Analysis a Simple Panel Response to Turbulent Boundary Layer, Air Force Report AFFDL-TR-67-81.

Kistler, A. L. and Chen, W. S. (1962), The Fluctuating Pressure Field in a Supersonic Turbulent Boundary Layer, Jet Propulsion Laboratory Report No. 32-277.

Kistler, A. L. (1959), Fluctuation Measurements in a Supersonic Turbulent Boundary Layer.

Kovasznay, L. S. G. and Chu, B. T. (1958), On the Fine Structure of Turbulence, *J. Fluid Mech.*

Kraichnan, R. H. (1956), Pressure Fluctuations in Turbulent Flow over a Flat Plate, *J. Acoustic Soc. Amer.*, Vol. 28.

Kraichnan, R. H. (1957), Noise Transmission from Boundary Layer Pressure Fluctuations, *J. Acoustic Soc. Amer.*, Vol. 29, No. 1.

Kuo, E. Y. T. (1965), On the Generation of Surface Roughness by Turbulent Wind, Doctoral Disseration at University of Connecticut.

Laufer, J. (1964), Some Statistical Properties of the Pressure Field Radiated by a Turbulent Boundary Layer, *The Phys. of Fluids J.*, Vol. 7, No. 8.

Laufer, J. (1961), Aerodynamic Noise in Supersonic Wind Tunnel, *J. Aeronaut. Sci.*, Vol. 28, No. 685.

Laumann, E. A. (1967), Jet Propulsion Laboratory Wind Tunnel Facility, JPL Tech. Memo. 33-335.

Leehey, P. (1968), Trends in Boundary Layer Noise Research, AFOSR-UTIAS Symposium on Aerodynamic Noise, Toronto, Canada.

Lilley, G. M. and Hodgson, T. H. (1960), On the Surface Pressure Fluctuation in Turbulent Boundary Layer, AGARD Report No. 276.

Lin, Y. K. (1967), Probabilistic Theory of Structural Dynamics, Chapter 7, McGraw-Hill, Inc., New York.

Lyamshev, L. M. (1961), Sound Radiation from Elastic Shells Excited by Turbulent Aerodynamic Flow, *Soviet Phys. Acost.*, Vol. 7, No. 1.

Lyon, R. H. (1957), Response of String to Random Noise Field, *JASA 28.*

Maestrello, L. (1965), Measurement and Analysis of the Response Field of Turbulent Boundary Layer Excited Panels, *J. Sound and Vibration,* Vol. 2, No. 3.

Maestrello, L. (1967), Use of Turbulent Model to Calculate the Vibration and Radiation Responses of a Panel, with Practical Suggestions for Reducing Sound Level, *J. Sound Vibration,* Vol. 5, No. 3.

Maestrello, L., Gedge, M. R. and Reddaway, A. R. F. (1967), Response of Structure to the Pseudo-Sound Field of a Jet (Using a Combined Continuum and Finite Element Method), Boeing Scientific Research Laboratories Document D1-82-0652.

Maestrello, L. (1968), Design Criterion of Panel Structure Excited by Turbulent Boundary Layer, *Journal of Aircraft,* Vol. 5, No. 4.

Maestrello, L. and McDaid, E. P. (1968), Sound Radiation from a Panel Excited by a Turbulent Boundary Layer, Boeing document (to be issued).

Maidanik, G. (1966), The Influence of Fluid Loading on the Radiation from Orthotropic Plates, *J. Sound Vib.*, Vol. 3, No. 3.

Meecham, W. L. (1965), Surface and Volume Sound from Boundary Layers, *J. Acoust. Soc. Amer.*, Vol. 37, No. 3.

Phillips, O. M. (1955), On Aerodynamic Surface Sound, Aero. Res. Council (London), Report No. FM 2094.

Phillips, O. M. (1960), On the Generation of Sound by Supersonic Turbulent Shear Layers, *J. Fluid Mech.*, Vol. 9, Part 1.

Powell (1960), Aerodynamic Noise and the Plane Boundary, *J. Acoust. Soc. Amer.*, Vol. 32, No. 8.

Pretlove, A. J. (1964), Free Vibrations of a Rectangular Panel Backed by a Closed Rectangular Cavity, *J. Sound Vib.*, Vol. 2, No. 3.

Ribner, H. S. (1956), Boundary Layer Induced Noise in the Interior of Aircraft, UTIA Rep. No. 37.

Schloemer, H. H. (1966), Effects of Pressure Gradients on Turbulent Boundary Layer Wall Pressure Fluctuations, U.S. Navy Underwater Sound Laboratory Report No. 747.

Serafini, J. S. (1963), Wall Pressure Fluctuations and Pressure Velocity Correlation in a Turbulent Boundary Layer, NASA TR-R-165.

Strawderman, W. A. (1967), The Acoustic Field in a Closed Space Behind a Rectangular Simply Supported Plate Excited by Boundary Layer Turbulence, USL Report No. 827.

Warburton, G. B. (1954), The Vibration of Rectangular Plates, *Proc. Inst. Mech. Engrs.*, Vol. 168, London.

Watson, R. D. and Cary, A. M. (1967), Transformation of Hypersonic Turbulent Boundary Layers to Incompressible Form, *AIAA Journal*, Vol. 5, No. 6.

White, P. H. and Cottis, M. G. (1968), Acoustic Radiation from a Plate-Rib System Excited by Boundary Layer Turbulence, Measurement Analysis Corporation, 702-06.

Wilby, J. F. (1966), The Response of Panels in Turbulent Boundary Layer Excitation, Ph.D. Thesis, University of Southampton.

Willmarth, W. W. and Wooldrige, C. E. (1963), Measurements of the Correlation between Fluctuating Velocities and the Fluctuating Wall Pressure in a Thick Turbulent Boundary Layer, AGARD Report No. 456.

Wills, J. A. B. (1968), Spurious Pressure Fluctuations in Wind Tunnels, *J. Acoust. Soc. Amer.*, Vol. 43, No. 5.

Wilson, L. N. (1959), An Experimental Investigation of the Noise Generated by Turbulent Flow around a Rotating Cylinder, UTIA Report No. 57.

Young, D. (1950), Vibration of Rectangular Plates by the Ritz Method, *ASME Trans.*, Vol. 72.